

Recurrence of Travelling Waves in Transitional Pipe Flow

By R. R. KERSEWELL¹ AND O. R. TUTTY²

¹Department of Mathematics, University of Bristol, Bristol BS8 1TW, UK

²School of Engineering Sciences, University of Southampton, Southampton, SO 17 1BJ, UK

(Received 2 February 2022)

The recent theoretical discovery of families of travelling wave solutions in pipe flow (Faisst & Eckhardt 2003; Wedin & Kerswell 2004; Hof et al. 2004) at Reynolds numbers lower than the transitional range naturally raises the question of their relevance to the turbulent transition process. Here a series of numerical experiments are conducted in which we look for the spatial signature of these travelling waves in transitional flows. Working within a periodic pipe of $5D$ (diameters) length, we find that travelling waves with low wall shear stresses (lower branch solutions) are on a surface which separates initial conditions which uneventfully relaminarise and those which lead to a turbulent evolution. Evidence for recurrent travelling wave visits is found in both $5D$ and $10D$ long periodic pipes but only for those travelling waves with low-to-intermediate wall shear stress and for less than about 10% of the time in turbulent flow. Given this, it seems unlikely that the mean turbulent properties such as wall shear stress can be predicted as an expansion over the travelling waves in which their individual properties are appropriately weighted. Rather, further dynamical structures such as periodic orbits need to be isolated and included in any such expansion.

1. Introduction

Wall-bounded shear flows are of tremendous practical importance yet their transition to turbulence is still poorly understood. Typically, the laminar flow solution is linearly stable (e.g. plane Couette flow, pipe flow) or if linearly unstable only well beyond the regime where transition occurs (e.g. channel flow). As a result, transition is an abrupt process triggered by a perturbation of sufficient amplitude. Generically, this could be expected to lead to an intermediate state of reduced symmetry but in fact the flow always immediately becomes temporally and spatially complicated. A recent new direction in rationalising this phenomenon revolves around identifying alternative solutions (beyond the laminar state) to the governing Navier-Stokes equations. In the past few years, such solutions in the form of steady states or travelling waves have been found in plane Couette flow (Nagata 1990; Clever & Busse 1992, 1997; Wale 1998), channel flow (Itano & Toh 2001; Wale 2001, 2003), an autonomous wall flow (Jimenez & Simens 2001) and most recently pipe flow (Faisst & Eckhardt 2003; Wedin & Kerswell 2004). Invariably, these solutions are saddle points in phase space. The idea is that through their stable and unstable manifolds and interconnections between them together with the appearance of periodic orbits, phase space becomes sufficiently complicated to support ‘turbulent’ trajectories.

Gathering supporting evidence for this scenario is in its infancy especially for spatially-extended systems but progress is being made. Eckhardt and coworkers have been central in applying such dynamical systems ideas to transition to turbulence (e.g. Schmiegel & Eckhardt (1997); Eckhardt et al. (2002); Faisst & Eckhardt (2004); Eckhardt et al. (2007)). Their basic approach has been to focus on the statistics of many transition events rather than specific examples and so far have been reasonably successful in rationalising the properties of reduced numerical models with known dynamical system structures in phase space (see Eckhardt et al. (2007) for a nice review). Complementary work has concentrated on establishing connections between specific flow behaviour and underlying nonlinear solutions present. In channel flow, for example, Itano and Toh (Itano & Toh 2001) interpret wall turbulent bursting events with flow along the unstable manifold of a travelling wave solution. They also managed to isolate a periodic-looking solution on the basin boundary of the turbulence by continually adjusting a trajectory such that it neither relaminarised or became turbulent (Toh & Itano 2003) (see Skufca et al. (2006) for an equivalent calculation in a model system). Jimenez et al. (Jimenez et al. 2005) studied both channel flow and plane Couette flow in an effort to relate near-wall turbulent events to the large number of known nonlinear solutions. They concluded that the turbulence stayed close to the upper branch travelling waves as far as comparing simple statistics of the flow field such as maximum (over space) wall-normal and streamwise components were concerned. Other work has focussed upon identifying isolated periodic solutions directly from numerically-integrated turbulent trajectories using a Newton-Raphson technique. In both the case of plane Couette flow Kawahara & Kida 2001) and highly-symmetric forced box turbulence (van Veen et al. 2006), the authors claim to find one periodic orbit which seems to share the same mean properties as the turbulent attractor.

In pipe flow, the only work so far aiming to establish the physical relevance of the recently-discovered travelling waves has been experimental (Hof et al. 2004, 2005). By analysing the flow structure across turbulent pipe flow (both of ‘pu’ and ‘slug’ type – see Wignanski & Champagne (1973)), good correspondence was found, at least occasionally, with the outer symmetrically-arranged ring of fast ‘streaks’ (streamwise velocity anomalies) which is one of the dominant features of the travelling waves. The match is less clear, however, with regards to the complementary slow streaks centred around the pipe axis as well as with the smaller cross-stream velocities (e.g. Figs 2E and 2F of Hof et al. (2004)). The purpose of this paper is to build on this work by carrying out a detailed quantitative study which can explore how closely the travelling waves are reproduced or ‘visited’ in phase space and the frequency of such visits using direct numerical simulations. If it emerges that turbulent pipe flow can be understood as an effectively random switching between the neighbourhoods of these travelling waves then an appropriately weighted expansion across the ‘active’ travelling waves visited may provide a useful predictor of the turbulent flow properties. This presumes that some version of periodic orbit theory developed in low dimensional dynamical systems (e.g. Cvitanovic 1988; Artuso et al. 1990a,b)) may carry over to this very high (formally infinite) dimensional setting.

The structure of the paper is as follows. §2 begins by briefly describing the numerical method used to solve the Navier-Stokes equations before discussing reasonable measures chosen to quantify if, and how well, the flow approaches a travelling wave (TW) solution. There is a certain amount of arbitrariness in this choice because the TWs are fully nonlinear solutions not obviously orthogonal under any inner product. Hence some experimentation has been necessary before a final choice on the exact ‘correlation’ functions to evaluate made. Given also the fact that the TWs are parameterised continuously by their

axial wavelength (albeit over a finite range), it has been convenient to impose a strict periodicity in the pipe to discretise the TWs which can exist in the system. As a result, a periodic pipe of length $5D$ has been used for the majority of the results. Even then, 37 TWs of two-, three- and four-fold rotational symmetry about the axis can be found at a Reynolds number of 2400. These are briefly described in §3 together with their stability. In §4, we show numerical evidence that some of the TWs are visited but not all and for only part of the time. In §5, the statistical frequency of these visits is quantified by examining the correlation data from across a number of runs. Finally, a discussion follows in §6.

2. Formulation

2.1. Numerics

The Navier-Stokes equation and solenoidal condition for the flow of an incompressible, Newtonian fluid along a circular, straight pipe under the action of an imposed pressure gradient are

$$\partial_t u + u \cdot \nabla u + \frac{1}{r} \nabla p = \nu \nabla^2 u; \quad \nabla \cdot \mathbf{u} = 0; \quad (2.1)$$

where ν is the kinematic viscosity, p the pressure and ρ the constant density. Non-dimensionalising the system using U the mean axial speed and the pipe radius $D/2$ where D is the diameter gives rise to the Reynolds number $Re = UD/\nu = 2400$. A constant mass flow rate – or equivalently Re – is maintained along the pipe at all times. A numerical solution for the primitive variables (velocity and pressure) was developed in cylindrical coordinates $(s; \theta; z)$ using finite differences in the radial direction (s) and Fourier modes for θ and z . The time stepping was performed using the third-order Runge-Kutta scheme of Nitkin (2006).

Hereafter a quoted numerical resolution of $(N; M; K)$ corresponds to $N + 1$ equally-spaced radial points (i.e. a grid step of $1/N$ where $0 \leq s \leq 1$) and Fourier expansions in θ and z of wavenumbers $M = 2; \dots; M = 2$ and $(K = 2; \dots; K = 2) = L$ respectively where L diameters is the nominal length over which periodicity is imposed. As discussed below, the main choice of pipe length was $L = 5$: for this geometry a coarse grid was $(25, 32, 30)$, an intermediate grid $(50, 48, 40)$ and a fine grid $(50, 60, 60)$: equivalent grids in longer pipes were used (e.g. a fine $10D$ -grid was $(50, 60, 120)$).

In addition to checks of specific components of the code using analytic test solutions, a series of calculations was performed using as initial conditions a TW solution plus a perturbation in the form of the leading (unstable) eigenfunction. Good agreement was obtained for the growth of the disturbance and that predicted from the eigenvalue. Importantly, the code was also cross-validated with another time-stepping code based on velocity potentials (Willis & Kerswell 2006).

Commonly in studies of this type the grid is stretched in the radial direction as the highest resolution is required near the wall. However, here there was little difference between the results obtained with uniform and non-uniform grids. This is not surprising given the nature of the flow at the Reynolds number considered in this study, as can be seen in Figure 3 below.

2.2. Travelling Waves

The TWs so far identified (Faisst & Eckhardt 2003; W edin & Kerswell 2004) are arranged into symmetry classes of m -fold rotational symmetry about the axis and then continuously parametrised by their axial wavenumber across a finite range. TWs of 1-fold through to 6-fold symmetry have been found (Kerswell 2005) but only 2-, 3- and 4-fold TWs are currently known to exist below $Re = 2485$. Within each symmetry class, the TWs appear through saddle node bifurcations so that close to the saddle node point there is a well-defined upper and lower branch solution for a given wavenumber. For higher Re , the solution surfaces typically kink and fold back on themselves so that multiple pairs of branches can coexist at the same wavenumber (e.g. figure 10 of W edin & Kerswell (2004)).

Imposing a pipe periodicity immediately reduces the continuum of TWs present down to a discrete number which can fit into the pipe. This is a crucial simplification which means the matching procedure adopted below can monitor all the TWs available to the flow. The main choice of a 5D long pipe was a compromise between the need to keep the number of TWs to a manageable size (helped by a shorter pipe) and the need to have a dynamical system which could support turbulent behaviour at a value of Re where the TWs are fully resolvable (helped by a longer pipe). This pipe length has also been studied before (Eggels et al. 1994; Faisst & Eckhardt 2004) and sustained turbulence predicted for $Re > 2250$ (Faisst & Eckhardt 2004). This short length, of course, precludes capturing turbulent spatiotemporal features such as ‘puffs’ (W ygnanski & Champagne 1973) which typically extend over $20D$ but does allow an examination of ‘temporal’ turbulence which, when triggered, fills the whole pipe.

Figures 1 and 2 show the result of tracing out all the 2-, 3- and 4-fold solution branches in the friction factor-axial wavelength plane at $Re = 2400$ where the friction factor (Schlichting 1968) is defined as

$$f = \frac{1}{2D} \frac{dp}{dz} \frac{U^2}{2D} \quad (2.2)$$

with dp/dz being the mean pressure gradient. The curves are similar but less contorted at $Re = 2000$ (Kerswell 2005) and $Re = 2200$ (not shown). The vertical dotted lines drawn at axial wavenumbers $k = 0.625n$ where $n = 1, 2, \dots, 5$ indicate the TWs which fit in the pipe which is actually taken to be $L = 0.625 = 5/8$ diameters long. The m -fold symmetry class, the letter label and wavenumber are used to identify the TWs in what follows. For example, the TW with wavenumber 1.25 and lowest friction factor in figure 1 is the 3b.1.25 TW. For this pipe geometry and Re , there are 37 TWs (6 2-fold, 22 3-fold and 9 4-fold rotationally symmetric TWs) which can be numerically resolved and used to match against the flow.

2.3. Matching

As fully nonlinear solutions, the TWs do not possess any simple orthogonality with respect to an inner product. Therefore establishing when a directly numerically simulated flow, u_{NS} , approaches a chosen TW velocity field, u_{TW} , is not a straightforward case of projection. Given this, a number of ad-hoc ‘correlation’ functions were developed and tested to measure how close the flow comes momentarily to a TW. The basic approach was to construct an integral based on the velocity fields u_{NS} and u_{TW} over one wavelength $2\pi = 2D$ of the TW near the middle of the pipe. The correlation functions found most useful

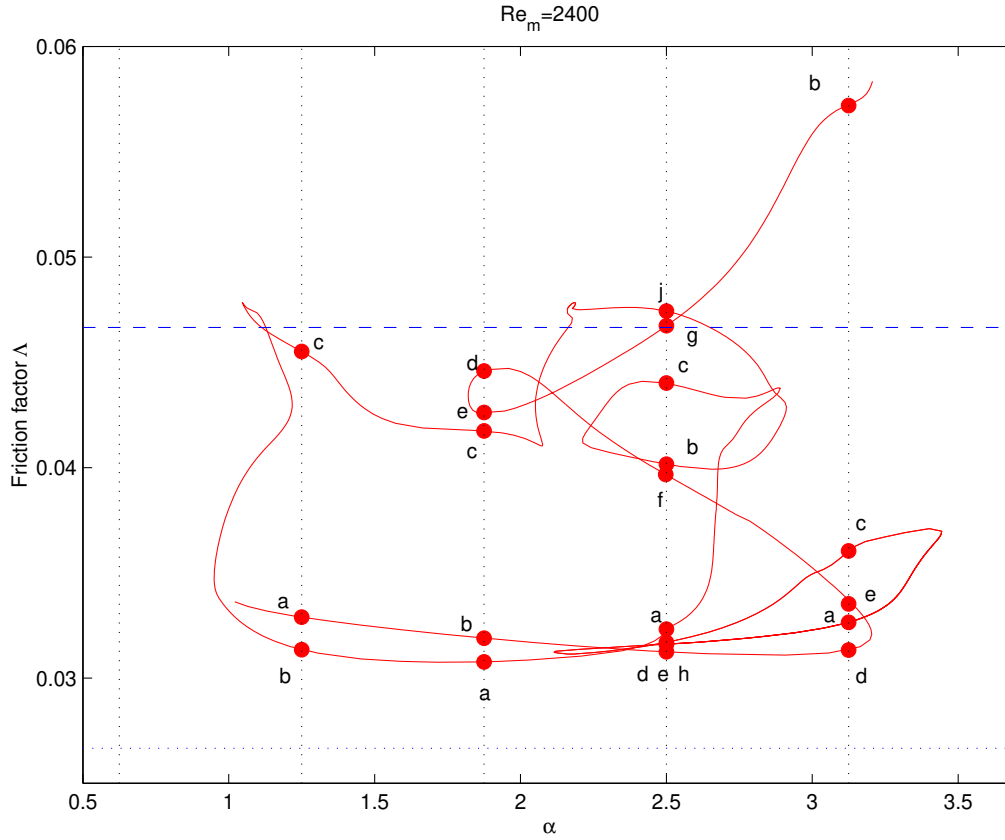


Figure 1. Solution branch for 3-fold rotationally-symmetric travelling waves plotted on a friction factor versus axial wavenumber plot at $Re = 2400$. The blue dotted line represents the lower bound given by the Hagen-Poiseuille solution ($\lambda = 64/Re$) and the upper blue dashed line corresponds to the $Re = 2400$ value of the log-law parameterisation of experimental data ($\lambda = 2.0 \log(Re_m)^{-0.8}$ (see Schlichting 1968 equation (20.30))). The solution branch is only shown as far as it is assured resolved (hence the loose ends: the main mapping resolution was (8;30;6) in the truncation nomenclature of W edin & K erswell 2004). The dotted vertical lines indicate the wavenumbers ($\alpha = 0.625n$ in units of $2\pi/D$, $n = 1;2;3;4;5$) which fit into a pipe of length $L = 0.625D$ long. The letters are used to label each allowable TW together with the wavenumber.

and thereby adopted were a normalised inner product based on the total velocity fields,

$$I_{\text{tot}}(t) = \max_{0 \leq z_0} \frac{\langle \mathbf{v}_{DNS}(s; z_0 + z) | \mathbf{v}_{TW}(s; z) \rangle}{\langle \mathbf{v}_{DNS}(s; z_0 + z) | \mathbf{v}_{DNS}(s; z) \rangle \langle \mathbf{v}_{TW}(s; z) | \mathbf{v}_{TW}(s; z) \rangle}; \quad (2.3)$$

once the mean profile of the TW

$$\bar{w}_{TW}(s) = \frac{1}{4} \int_0^2 \int_0^2 w_{TW}(s; z) dz \quad (2.4)$$

had been subtracted from both velocity fields

$$\begin{aligned} \mathbf{v}_{DNS} &:= \mathbf{u}_{DNS}(s; z_0 + z) - \bar{w}_{TW}(s)\mathbf{b} \\ \mathbf{v}_{TW} &:= \mathbf{u}_{TW}(s; z) - \bar{w}_{TW}(s)\mathbf{b} \end{aligned}$$

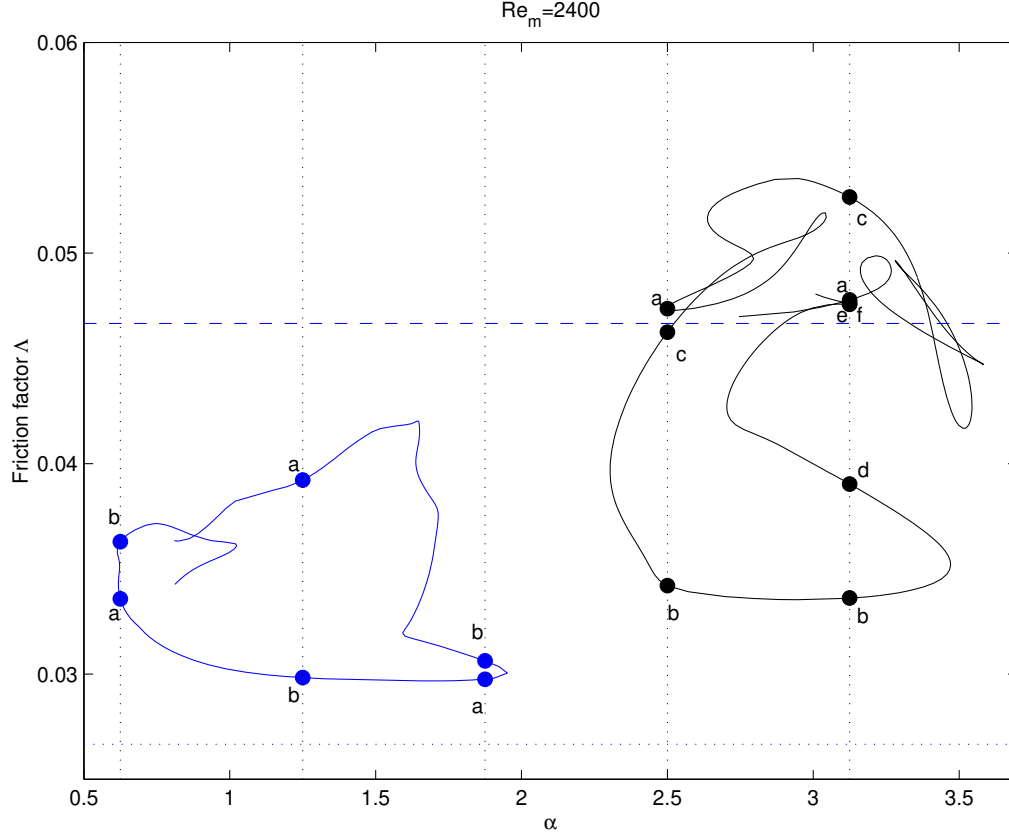


Figure 2. The equivalent of figure 1 but for the 2-fold (left, blue) and 4-fold (right, black) rotationally-symmetric travelling waves. Typical truncations used to resolve these solutions were (9;25;7) for the 2-fold case and (6;40;5) for the 4-fold case.

and an inner product using the cross-stream velocity components

$$I_{uv}(t) = \max_{0 \leq z_0} \frac{\int_{-Z_2}^{Z_2} \int_{-Z_1}^{Z_1} \mathbf{u}_{DNS}^2 \cdot \mathbf{u}_{TW}^2 \, d\mathbf{x}}{\int_{-Z_2}^{Z_2} \int_{-Z_1}^{Z_1} \mathbf{u}_{DNS}^2 \cdot \mathbf{u}_{DNS}^2 \, d\mathbf{x} \int_{-Z_2}^{Z_2} \int_{-Z_1}^{Z_1} \mathbf{u}_{TW}^2 \cdot \mathbf{u}_{TW}^2 \, d\mathbf{x}} : \quad (2.5)$$

Here $\mathbf{u}^2 = (u; v; 0)$ is the cross-stream velocity part of \mathbf{u} , and

$$\int_{-Z_2}^{Z_2} \int_{-Z_1}^{Z_1} \mathbf{u}_1 \cdot \mathbf{u}_2 \, d\mathbf{x} = \frac{1}{2\pi^2} \int_{-Z_2}^{Z_2} \int_{-Z_1}^{Z_1} \int_0^{2\pi} u_1 \cdot u_2 \, ds \, d\mathbf{x} \, dz \quad (2.6)$$

is the (usual) inner product.

The second measure I_{uv} is necessary as the TW streamwise (streak) velocities are typically an order of magnitude larger than the cross-stream velocities and hence their matching contribution tends to dominate I_{tot} , to the extent that there is little difference between I_{tot} and I_w (the equivalent of I_{uv} but using the streamwise velocity component only), even though the mean flow has been subtracted. A correlation using the full velocity fields \mathbf{v}_{DNS} and \mathbf{v}_{TW} is not a sensible measure as it is dominated by the mean streamwise flow to the extent that all correlations involving the axial velocity would be large.

By design, I_{tot} and I_{uv} can only take values in the interval $[-1;1]$ with a value 1 indicating a perfect match. The phase optimisation over ϕ_0 and z_0 (carried out by systematically evaluating all the options over the $[0;2\pi) \times [-\pi; \pi)$ grid) in practice ensured that the correlations were never very negative typically lying in the interval $[-0.2;0.2]$. Experience indicated that there is evidence for a TW visit if I_{tot} and I_{uv} reach values of 0.5 and above (although more on this below).

A number of other measures were tried. An inner product using the streamwise vorticity, which provides a single measure of the cross stream flow, was found to shadow I_{uv} , although at a lower level. The symmetry assumed for the TW's (see 2.7 below) ensures that the cross stream velocity is zero along the axis of the pipe. This would not be expected to occur over an extended length of the pipe in fully turbulent flow. Hence an inner product over a subset of the domain excluding the central portion could be suitable. This was investigated, and it was found that restricting the domain to $\frac{1}{2} \leq s \leq 1$ produced somewhat higher correlations, particularly for I_{uv} , but, again, a similar pattern of behaviour. Hence, these other measures could be used to produce essentially the same results by adjusting the level of correlation that would be regarded as giving a good match.

The matching was performed by maximising the value of I_{uv} over all possible values of ϕ_0 and z_0 . I_{tot} was then calculated for the same orientation. I_{tot} is not suitable as the primary measure as it is so heavily dominated by the streamwise component that the cross-stream structure of the flow would, in effect, be discounted when choosing the "best" match.

Some of the TW's are highly correlated (values greater than 0.95 have been observed), so that, at a specific time, using these measures, there can be a good match of the flow to more than one TW. In cases such as this, the value of the mean wall shear stress and the perturbation kinetic energy can be used to select the most appropriate match.

2.4. Travelling Wave Stability

An obvious way to start the DNS runs is to use a TW together with some small perturbation as an initial condition. If this perturbation is unstructured, for example, by relying on numerical discretization errors, the flow takes a long time to exit the neighbourhood of the TW and wastes cpu time. A better strategy is to find the unstable eigendirections of the TW and to use the most unstable eigenfunction with a small amplitude as the perturbation. Four 'lower' branch TWs - 2b_1.25, 3a_2.5, 3h_2.5 and 4b_3.125 - and four 'upper' branch TWs - 2a_1.25, 3b_3.125, 3j_2.5 and 4c_3.125 - were selected as starting TWs. The distinction between upper or lower branch solutions can be ambiguous when the solution surface is as convoluted as in figure 1. Here we consider that TWs with high friction factors are upper branch solutions and those with low friction factor are lower branch solutions. The 8 choices made represent extreme and therefore unambiguous examples under this categorisation.

The stability properties of the 8 chosen TWs are listed in Table 1. The travelling waves all possess the shift- & -reflect symmetry S

$$S : (s; \phi; z) \mapsto (s; \phi; z + \pi); \quad S : (u; v; w; p) \mapsto (u; -v; w; p); \quad (2.7)$$

so permitted linear disturbances can either be partitioned into those symmetric or antisymmetric with respect to S . When checked the TWs were invariably stable to an-

Branch	TW	Number of Unstable Eigenvalues	Largest Growth Rate (in units of U/D)	Resolution ($M; N; L$)
Lower	2b_1.25	1r	1:1 10^{-1}	(9,25,7)
	3a_2.5	2r	2:1 10^{-1}	(8,30,6)
	3h_2.5	3r+ 2c	1:7 10^{-1}	(8,30,6)
	4b_3.125	1r+ 2c	2:6 10^{-1}	(6,40,5)
Upper	2a_1.25	4c	6:6 10^{-2}	(9,25,8)
	3b_3.125	2c	3 10^{-3}	(8,30,5)
	3j_2.5	6c	1:7 10^{-1}	(8,30,6)
	4c_3.125	6c	3:7 10^{-1}	(6,40,5)

Table 1. The stability properties of typical upper and lower travelling waves at $Re = 2400$: r and c indicate the number of real and complex eigenvalues respectively. The resolution ($M; N; L$) is the same for the travelling waves and the stability calculation and indicates the azimuthal, radial and axial resolution respectively: see Wedin & Kerswell (2004) for details. The unstable eigenvalues all correspond to disturbances possessing the same shift- & -reflect symmetry as the travelling wave.

isymmetric disturbances so Table 1 concentrates exclusively on the situation in the S-symmetric subspace. The number of unstable directions is strikingly small given the large degrees of freedom involved (e.g. $O(15;000)$) and the size of the growth rates – $O(0.1 U=D)$ indicate inertial instabilities. Figure 3 shows the structure of the most unstable eigenfunctions for the lower branch TWs 2b_1.25 and 3a_2.5. The 3a_2.5 TW gives a particularly clear example of how an unstable eigenfunction is concentrated in the regions of maximum shear in the TW streak velocity.

3. Results

A series of runs were performed by taking as initial conditions each of the selected 8 upper and lower TWs perturbed by a small amount of their most unstable eigenfunction. Since this perturbation can be added or subtracted, 16 runs were in fact done. This protocol highlighted a fundamental difference between the upper and lower branch TWs. For all the lower branch TWs tested, starting the run in one sense along the TW's most unstable manifold invariably led to an uneventful gradual relaminarisation, whereas starting in the other sense always produced a turbulent evolution. Both signs of perturbation, in contrast, produced a turbulent trajectory for the upper branch TWs. This implies that the 4 lower branch TWs (and by implication other lower branch TWs) and their stable manifolds are part of a boundary dividing regions of phase space which lead to the two different types of behaviour. Their unstable manifolds are then either directed towards the laminar or turbulent states normal to this bounding surface. The terminology 'basin of attraction' and 'separatrix' has purposely been avoided here as the second initial observation when doing these runs at $Re = 2400$ with a 5D pipe is that the turbulence is only transitory. In other words, the laminar state is still the global attractor at $Re = 2400$ in a 5D periodic pipe although the flow can experience a long but ultimately finite turbulent episode. Not surprisingly, the length of these turbulent transients seems to depend sensitively on the exact numerical resolution used. This is particularly true

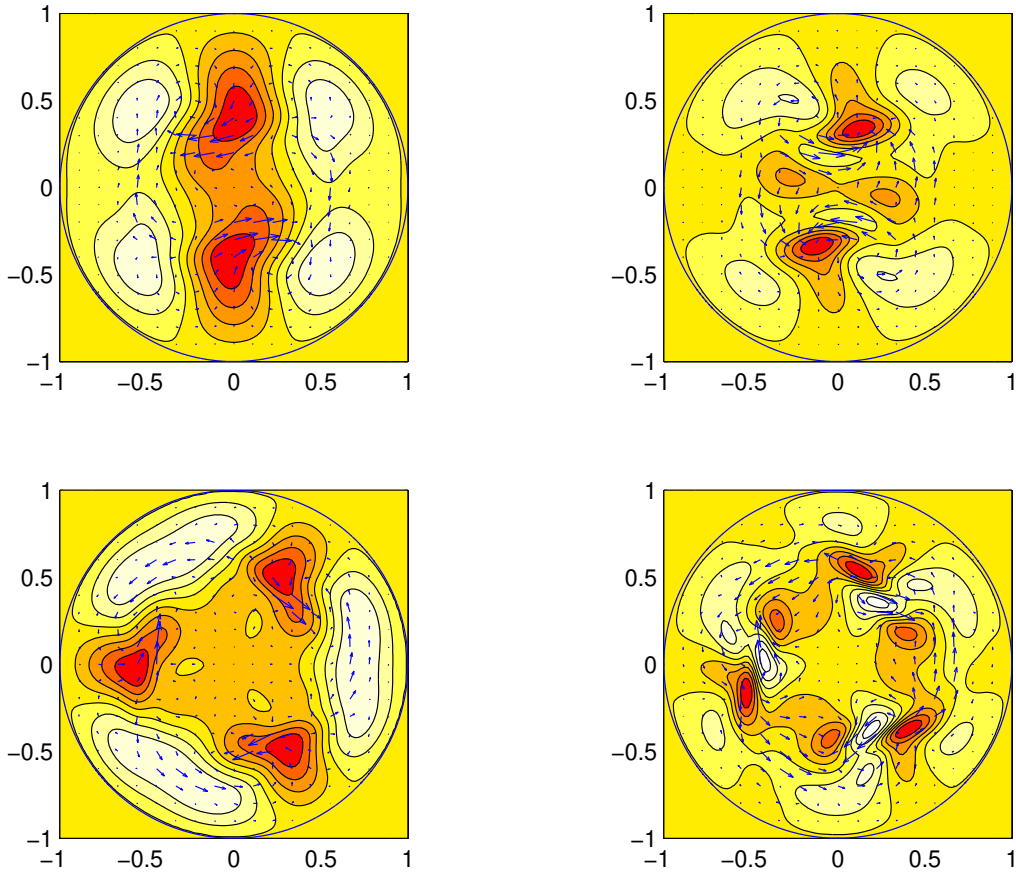


Figure 3. The travelling waves 2b.1.25 (top left) and 3a.2.5 (bottom left) and their most unstable eigenfunctions (top right for 2b.1.25 and bottom right for 3a.2.5). The arrows indicate the cross-stream velocities (larger arrows corresponding to larger speeds) for all 4 plots. The shading represents the axial velocity for the eigenfunctions whereas for the travelling waves, the axial velocity differential away from the laminar flow corresponding to the same mass flux is plotted (dark most negative – slow streaks – and light most positive – fast streaks). The same contour levels are used throughout with the eigenfunctions renormalised so that their largest axial velocity is set to the largest absolute contour level (the shading outside the pipe indicates 0: contours levels range from $-0.417U$ to $0.266U$ in 8 steps).

with regards to the azimuthal and axial resolution – reducing this too far can produce what looks to be sustained turbulence (e.g. turbulence remains transient when reducing the resolution from the working resolution (50;60;60) to (25;30;30) or (50;24;24) but looks to be sustained at (50;16;16) over a time greater than $3;000D = U$: the resolution of Faisst & Eckhardt (2004) which predicts sustained turbulence at $Re = 2250$ is somewhere in between these last two choices). The issue of exactly when (or indeed if!) pipe flow turbulence becomes sustained is an area of much current interest at the moment (Peixinho & Mullin 2006; Hof et al. 2006; Willis & Kerswell 2006).

The two runs started around the lower branch TW 4b.3.125 illustrate the general

behaviour well. Figure 4 plots the kinetic energy (per unit mass)

$$KE := \frac{1}{2L} \int_0^{Z_{2L}} \int_0^{Z_2} \int_0^{Z_1} \frac{1}{2} (u - u_{lam})^2 ds dz \quad (3.1)$$

of the flow beyond the laminar state versus the mean wall shear stress

$$\tau = \frac{1}{2LD} \int_0^{Z_{2L}} \int_0^{Z_2} \frac{\partial w}{\partial s} dz \quad [= \frac{1}{8} U^2 = \frac{1}{16} Re (2U^2 = Re)] \quad (3.2)$$

for the flow evolution together with all 37 of the TWs present. Strictly when comparing with values for a TW, the kinetic energy and mean wall shear should be calculated for the section of the pipe containing the best match. However, for a pipe of this length, flow structures tend to persist over the full length of the pipe, particularly in the near wall region containing the streaks. The wall shear stress depends only on the streamwise velocity, which also provides the dominant component of the kinetic energy perturbation. As a result, there is usually little difference in these quantities for the full pipe and a section corresponding to one of the travelling waves. Larger differences were observed in longer pipes.

For one sign of the eigenfunction perturbation, the flow tamely relaminarises while for the other it executes a long turbulent transient. During this latter evolution, there is evidence of close visits to at least 5 TWs. The first (labelled '1' in figure 4) is to 4f_3:125 and occurs during the early stages as the flow trajectory moves away from 4b_3:125; see figure 5. This quality of the match is extremely high suggesting that there may be a heteroclinic connection between the two TWs. The fact that even at $t = 0$ there is already a considerable correlation with 4f_3:125 indicates that 4b_3:125 is structurally similar to 4f_3:125, an observation which is also true for some other groupings of TWs within the same rotational symmetry class. Figure 5 also shows the correlation signal for 4c_3:125 which has a very close visit after $120 D = U$ (labelled '4'). Taken together, the correlation functions for the other 4-fold TWs indicate that the flow retains its 4-fold symmetry until about $130 D = U$ (this was verified by examining the transient solution), whereupon it switches to a predominantly 3-fold symmetry. Figure 6 shows this switch-over well via the correlation function I_{tot} for 3a_3:125. This TW is the best candidate for a close visit (labelled '5' at $t = 250 D = U$) over all the 3-fold symmetric TWs. Figure 7 shows how the contribution to the correlation functions vary over the matching wavelength at point '5'. The total correlation I_{tot} is uniformly high but I_{uv} is low indicating that there is probably a good match in the streak structure but not in the cross-stream velocities. This is confirmed in figure 8 where there is clear evidence of 3 equally-spaced fast streaks around the outside of the pipe like 3a_3:125 which are fairly streamwise independent. Surprisingly, there is little similarity between the inner slow streak structures. The axial vorticity is a convenient but particularly discriminating way of probing the cross-stream velocity fields as it involves taking derivatives. Given the low value of I_{uv} , the poor comparison is expected however there is evidence that the DNS flow and the TW have roughly the same wavelength of variation.

During the dominantly 4-fold symmetric phase, there is also evidence for visits to 2b_0:625 and 2a_1:25 (labelled '2' and '3') shown in figure 9. A further way to characterise the extent of all these visits is to compare the kinetic energy and wall shear stress of the flow across the length of the pipe used for matching with the values associated with the TW. This data is collected together in figure 4. The relative closeness of these points to the corresponding values for the TW (e.g. '5' and 3a_3:125) is further support-

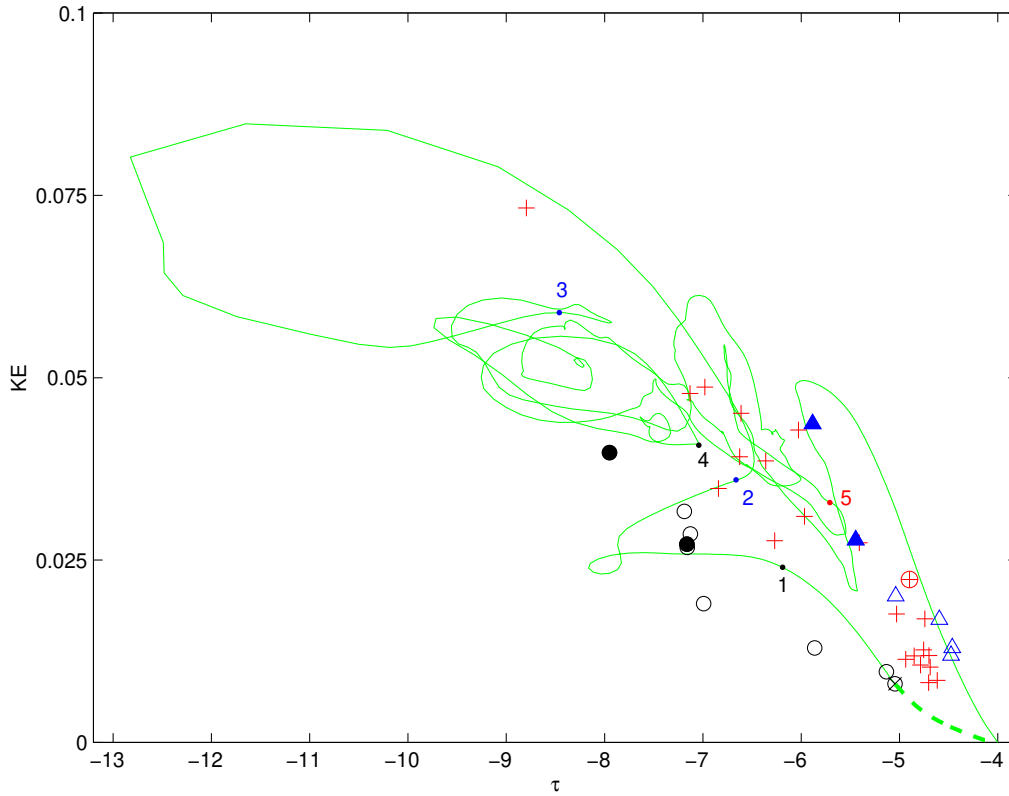


Figure 4. The surplus kinetic energy per unit mass, in units of U^2 versus wall shear stress in units of $2U^2 = Re$ for u_{DNS} starting at TW $4b_3:125$ (marked as a cross with a \cdot). The solid line indicates the turbulent evolution for one sign of the eigenvalue perturbation and the thick dashed line traces out the uneventful relaminarisation for the other (respectively $4b_3:125$ ($\pm =$)). The laminar state is represented by the point $(4;0)$. All the TWs present are also plotted: \cdot for 2-fold TWs, $+$ for 3-fold TWs and \triangle for 4-fold TWs. Filled in symbols indicate TWs which appear to be visited by u_{DNS} and the numbered dots indicate the temporal points of closest approach. In chronological order: 1 – $4f_3:125$ (lower black filled circle); 2 – $2b_0:625$ (blue filled triangle furthest from 3); 3 – $2a_1:125$ (closer blue filled triangle); 4 – $4c_3:125$ (upper black filled circle) and 5 – $3a_3:125$ (circled red $+$).

ing evidence of a visit.

Runs started at upper branch TWs with either sign of unstable eigenfunction lead to turbulent-looking trajectories. Figure 10 shows one of these runs starting with $3b_3:125$. Just as in the case of $4b_3:125$, the initial rotational symmetry of the flow lingers for a substantial time. During this phase, there is clear evidence of close visits to $3b_2:5$, $3c_2:5$ and $3j_2:5$ (see figure 11). The first visit is particularly significant as the structural overlap between the initial TW ($3b_3:125$) and the visited TW ($3b_2:5$) is low: by point 1', both I_{tot} and I_{uv} for $3b_2:5$ have risen from 0.4 to near 0.8 in just over $50D = U$. Figure 12, which compares the initial condition, the DNS flow at point 1' and the TW $3b_2:5$, confirms that the flow makes a significant adjustment to match with the new TW.

After a time of about $125D = U$ – see Figure 13 – the flow switches to being more 2-fold symmetric. The flow then successively visits $2a_1:125$ and $2b_1:875$ before relaminarising

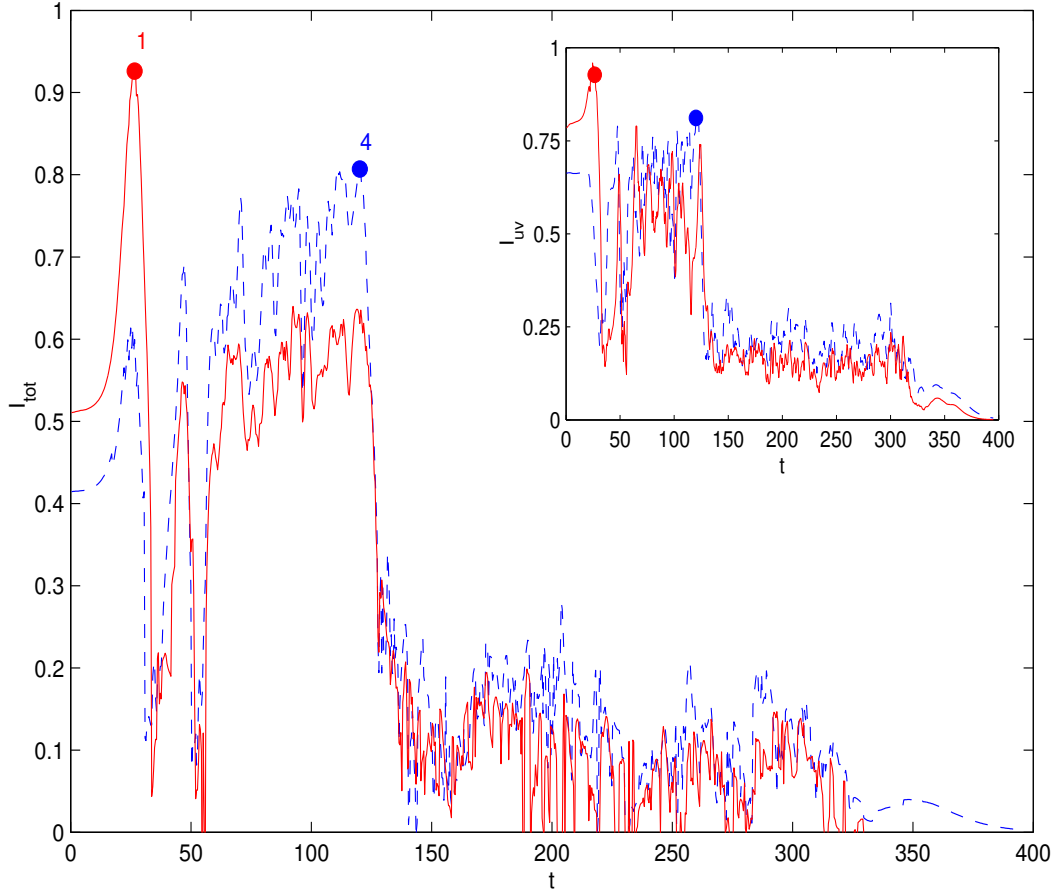


Figure 5. I_{tot} and I_{uv} (inset) as a function of time for TWs 4f_3:125 (red solid line) and 4c_3:125 (blue dashed line) starting at TW 4b_3:125. Dots label the times of likely closest visits to each TW (times 1' and 4' coincide with those in Figure 4).

at a time $350 D = U$. Point 4 gives a very good comparison between the the DNS flow and the TW 2a_1:25 because the correlation functions I_{tot} and I_{uv} are simultaneously large within the comparison wavelength: see Figure 14 at $z = 1.5$. The velocity plots – see Figure 15 – are very similar even up to the same vortex in the top left quadrant of the cross-sectional snapshots.

In Figure 10 point 5 is tagged as a match to TW 2b_1:875 as this TW has the largest correlation to the flow at this point, with $I_{tot} = 0.63$ and $I_{uv} = 0.61$. However, this is not the only TW that satisfies the criterion for a good match. Specifically, TW 2a_1:25 has $I_{tot} = 0.58$ and $I_{uv} = 0.49$. Also, 2a_1:25 is closer to point 5 than 2b_1:875 in Figure 10. That both of these TW's show a high correlation with the flow is not surprising as the TW's also show a high correlation (matching 2b_1:875 to 2a_1:25 gives $I_{tot} = 0.53$

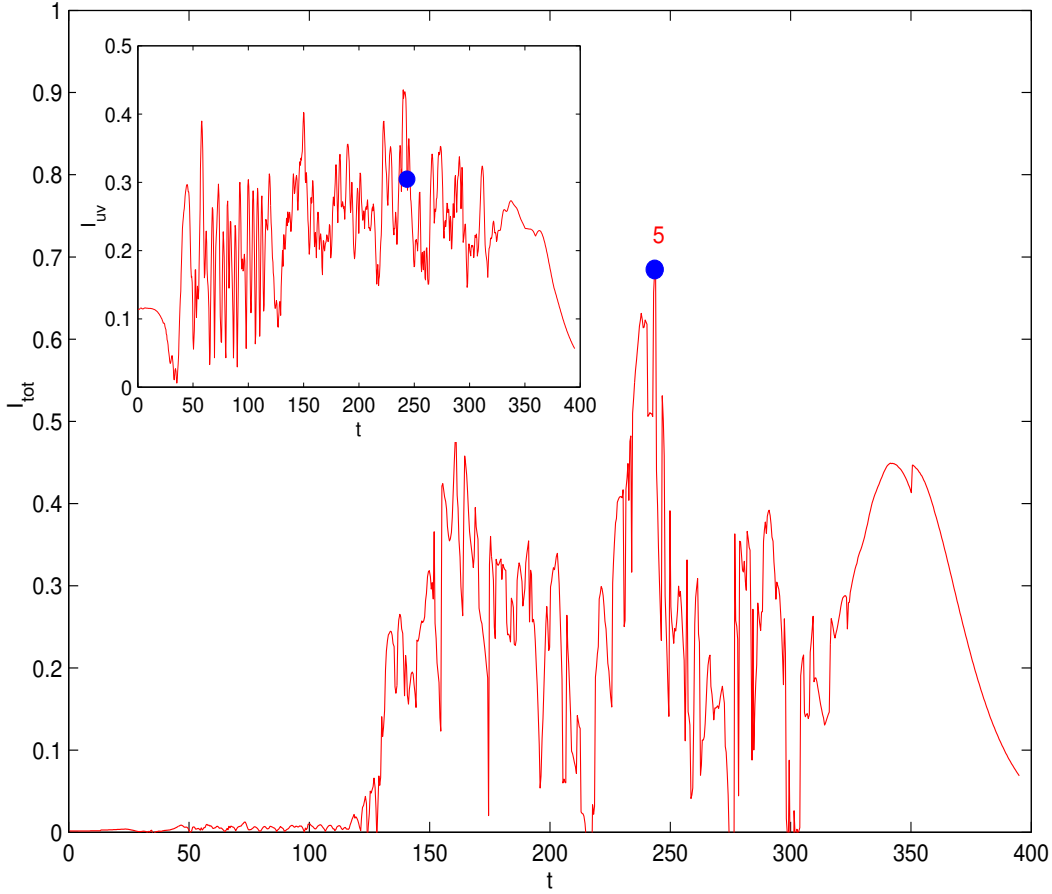


Figure 6. I_{tot} and I_{uv} (inset) as a function of time for TW 3a_3:125 starting at TW 4b_3:125. The dot labels the time of closest visit (corresponding to 5' in figure 4).

and $I_{uv} = 0.62$). Figure 16 shows a comparison between the flow at point 5 and the two travelling waves. In general, Figure 16 suggests that there is better agreement between TW 2a_1:25 and the flow than 2b_1:875, despite the fact that it has a lower correlation as measured by I_{tot} and I_{uv} . That this can occur is not unexpected since I_{tot} and I_{uv} are measures of shape and not amplitude. Figure 16 and the position of the TW's on 10 suggests there is a better agreement in amplitude between 2a_1:25 and the flow than with 2b_1:875.

No significant correlations were found with any 4-fold TWs as the correlation functions $I_{tot} = 0.3$ and $I_{uv} = 0.45$ throughout the evolution. This was a persistent finding in all the other runs where a 2-fold or 3-fold symmetric TW was used to initiate the flow. Even when the flow was started by a 4-fold symmetric TW, correlations with other 4-fold symmetric TWs would only be significant in the initial phase of the flow evolution.

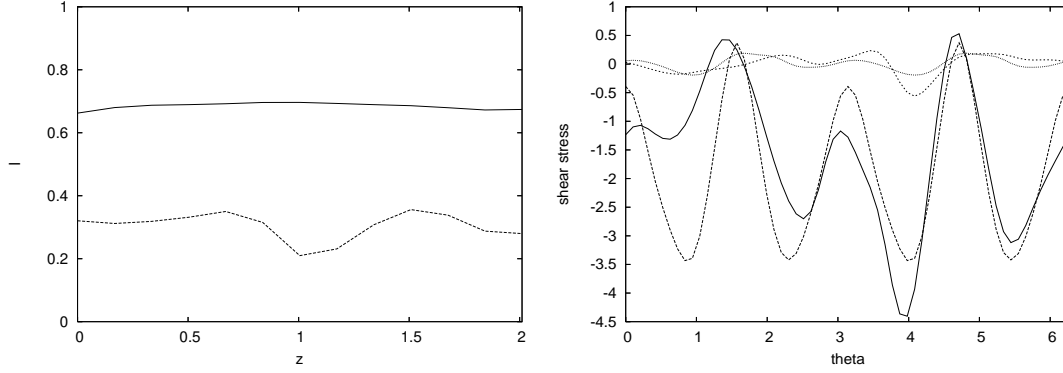


Figure 7. The left plot shows the correlations I_{tot} (upper line) and I_{uv} (lower line) over one wavelength of TW $3a_{3:125}$ at point 5 in Figure 6. The right plot shows the azimuthal distribution of the wall shear stress in units of $2U^2/Re$ at the axial position of maximum $I_{tot} + I_{uv}$ near $z = 1.5$. The upper lines give the azimuthal stress and the lower lines the axial stress (minus the laminar value of -4). The regular lines with 3-fold symmetry are for the TW and the more irregular ones from the DNS values.

where the seeding symmetry is still present. In contrast, certain 2-fold and 3-fold TWs were consistently visited regardless of how the flow was initiated. The fact that the 4-fold symmetric TWs have a higher wall-shear-stress-to-kinetic-energy ratio than the flow seems to adopt is indicated by Figures 4 and 10 and equivalent plots for other starting TWs (not shown). The flow never seems to visit the part of phase space where the 4-fold TWs are unless specially inserted whereas some of the 2-fold and 3-fold symmetric TWs are in the active part of phase space populated by turbulent trajectories.

Information about which TWs are visited in each of the 12 turbulent runs is summarised in Tables 2 and 3. The criterion used to indicate a visit is $I_{tot} > \epsilon$ and $I_{tot} + I_{uv} > 2$ with $\epsilon = 0.5$ and $\epsilon = 0.6$ for a closer visit. There is a strong correlation between the rotational symmetry of the starting TW and the waves subsequently visited even when the initial transient – defined as the period when I_{tot} for the initial TW decreases (typically of $O(30D/U)$ in duration) – is not considered. For instance, runs 1, 2, 5 and 10 – see Table 2 – show no evidence of visits to TWs with different rotational symmetry. However, across this suite of runs, all the TWs are visited at least once except for the 3 TWs $3a_{1:125}$, $3b_{1:125}$ and $3c_{1:125}$. Table 3 shows the more discerning results of only considering times when the flow leaves the rotational symmetry class of the initial TW. Examples of when this occurs have already been discussed in run 4 (at about $130D/U$; see Figure 6) and in run 7 (at about $125D/U$; See Figure 13). This makes it particularly clear that the 4-fold rotationally symmetric TWs are never visited except when the run is specially started near one of these TWs (runs 4, 11 and 12) whereas 2-fold and 3-fold symmetric TWs are visited regardless of the starting symmetry (e.g. runs 3, 6, 7, 9).

3.1. Frequency of Visits

Given the evidence above that the TWs are visited, the next question is how frequently. To answer this, ‘visit’ statistics were compiled across a number of different runs which

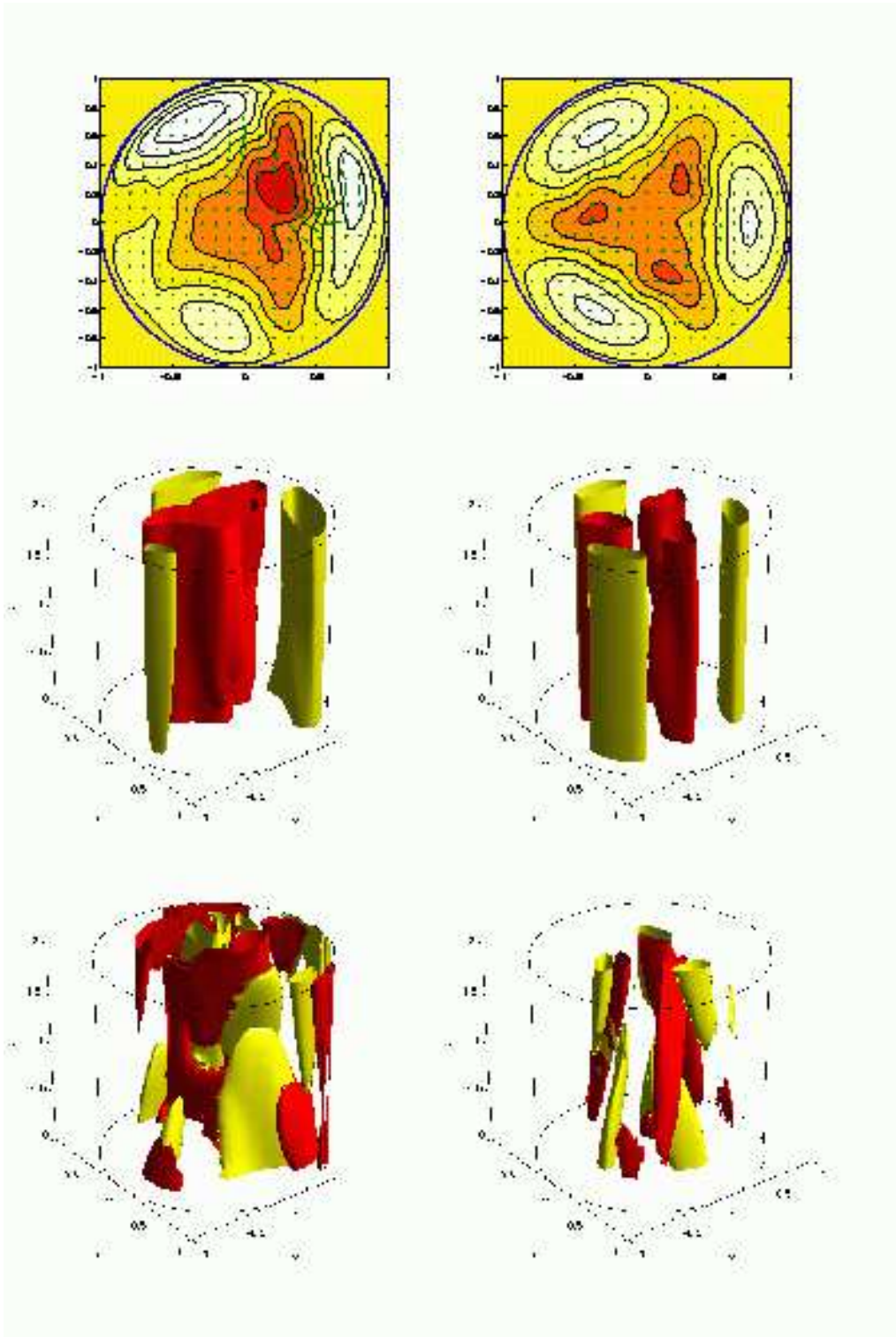


Figure 8. Comparison plots of the DNS flow (left column) and the TW $3a_3:125$ (right column) at point 5 in Figure 6. The top row shows the velocity fields at the streamwise position of maximum $I_{tot} + I_{uv}$ shown in Figure 7. (CHECK) The shading represents the axial velocity perturbation from laminar flow with contours from -0.55 (dark) to 0.5 (light) for the DNS, and -0.4 to 0.35 for the TW, with a step of 0.15 . The arrows indicate the cross stream velocity, scaled on magnitude (maximum $0.15U$). The middle row shows the streak structure over the wavelength of the TW, with contours of axial velocity at $0.3U$ (light/dark). The bottom row shows the axial vorticity, with contours at $0.6U=D$ (light/dark).

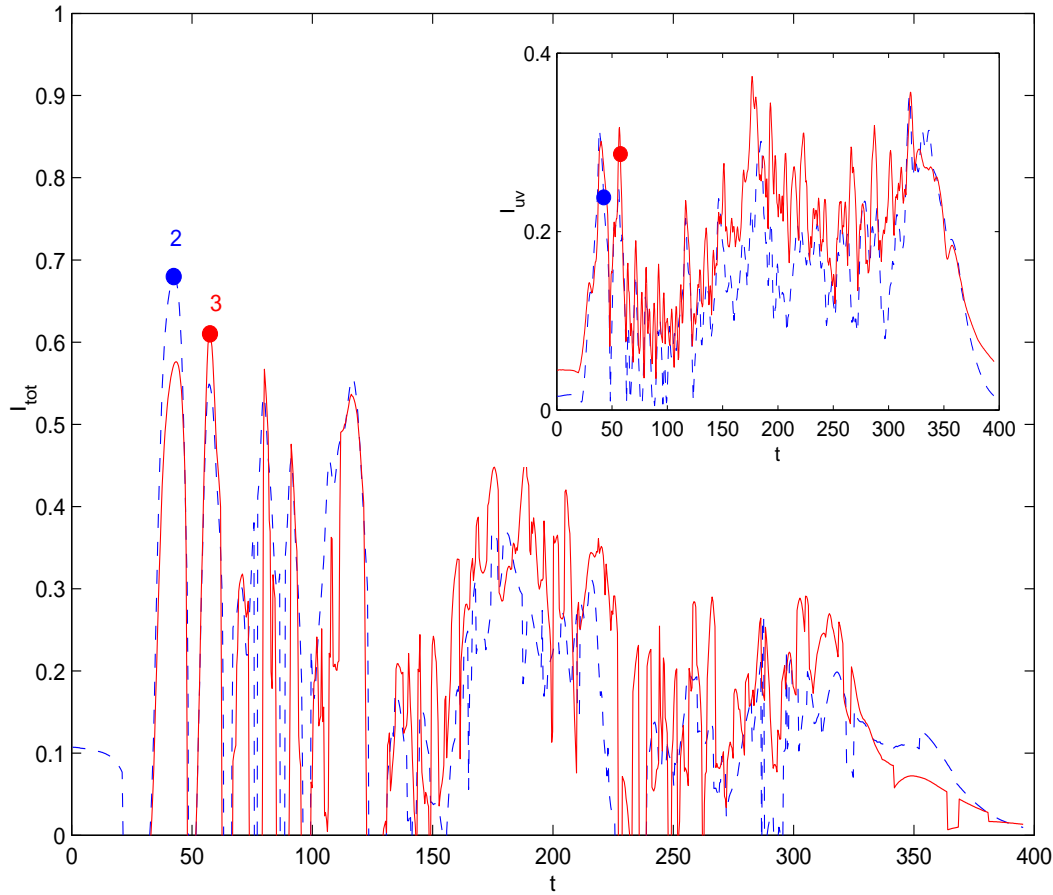


Figure 9. I_{tot} and I_{uv} (inset) as a function of time for TWs 2b_0:625 (blue dashed line) and 2a_1:25 (red solid line) starting at TW 4b_3:125. Dots label the times of likely closest visits to each TW (times 2' and 3' coincide with those in figure 4).

exhibited turbulent episodes. Ideally, these should be composed from one very long – e.g. $O(10,000 D = U)$ – turbulent run but, as discussed already, none could be generated at this Re where the TWs are available. As a result, two strategies at quantifying the TW visit frequency were undertaken. The first involved piecing together all the turbulent episodes produced during the suite of 5D runs described above. The second was to generate longer turbulent data sets in a double-length 10D pipe; for relatively short pipes, the length of pipe appears to have a significant effect of the time turbulence is sustained for, as can be seen from Table 4. These latter runs were almost exclusively initiated by randomly-selected velocity fields taken from a long turbulent coarse-grid run: see Table 4. The coarse grid is too underresolved to reproduce the TWs accurately and hence calculate correlation functions directly but was perfectly adequate to initiate turbulence in

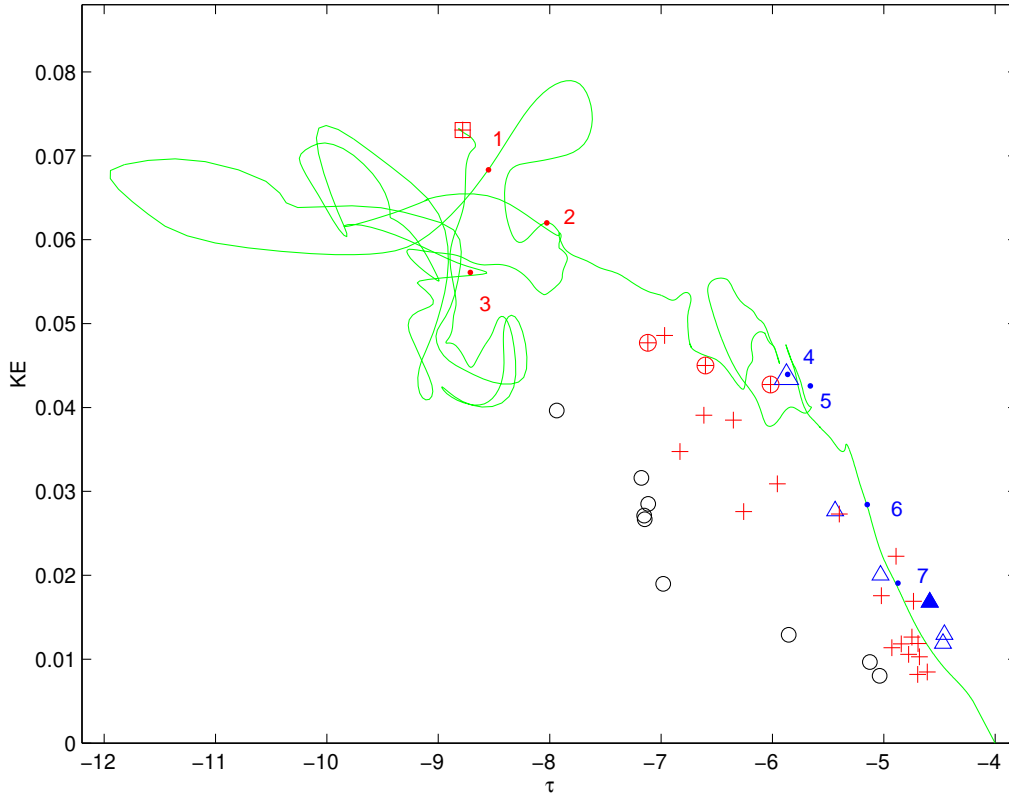


Figure 10. The surplus kinetic energy per unit mass in units of U^2 versus wall shear stress in units of $2U^2/Re$ for u_{DNS} starting at the upper branch TW 3b.3.125 (+) (marked as a with a + in it). The laminar state is represented by the point $(-4; 0)$. All the TWs present are also plotted: 4 for 2-fold TWs, + for 3-fold TWs and for 4-fold TWs. The numbered dots indicate the temporal points of closest approach. In chronological order: 1 - 3b.2.5 (rightmost red circled +); 2 - 3j.2.5 (leftmost red circled +); 3 - 3c.2.5 (middle red circled +); 4 and 6 - 2a.1.25 (large blue triangle); 5 and 7 - 2b.1.875 (blue solid triangle).

ner grid runs.

For the 5D runs started at a TW, it was necessary to decide when the flow had left the neighbourhood of the TW and had started to behave in a turbulent fashion. Two different criteria were adopted for this. In the first (data set A), the start of the turbulent phase was taken as the time at which the correlation with the starting TW had reached a minimum. This turned out to be more stringent a criterion (i.e. produced a later time) than requiring that the flow trajectory merely enter the part of the KE plane occupied by the turbulent state. In the second (data set B), the start of the turbulent phase was taken as when the flow broke out of the initial rotational symmetry class of the starting TW (e.g. for run 4 this occurs at about $130 D = U$; see Figure 6). In both cases the end of the turbulent phase was well estimated by when the flow trajectory left this 'turbulent' KE area. The subsequent relaminarisation phase was easily identified with both the perturbation kinetic energy and wall stress decaying monotonically down to their laminar values (e.g. see figures 4 and 10). These strategies produced a correlation data sets lasting $4;154 D = U$ (A) and $2;363 D = U$ (B). For each, a joint probability density function was then computed for I_{tot} and I_{uv} corresponding to the TW with largest I_{tot} at a given

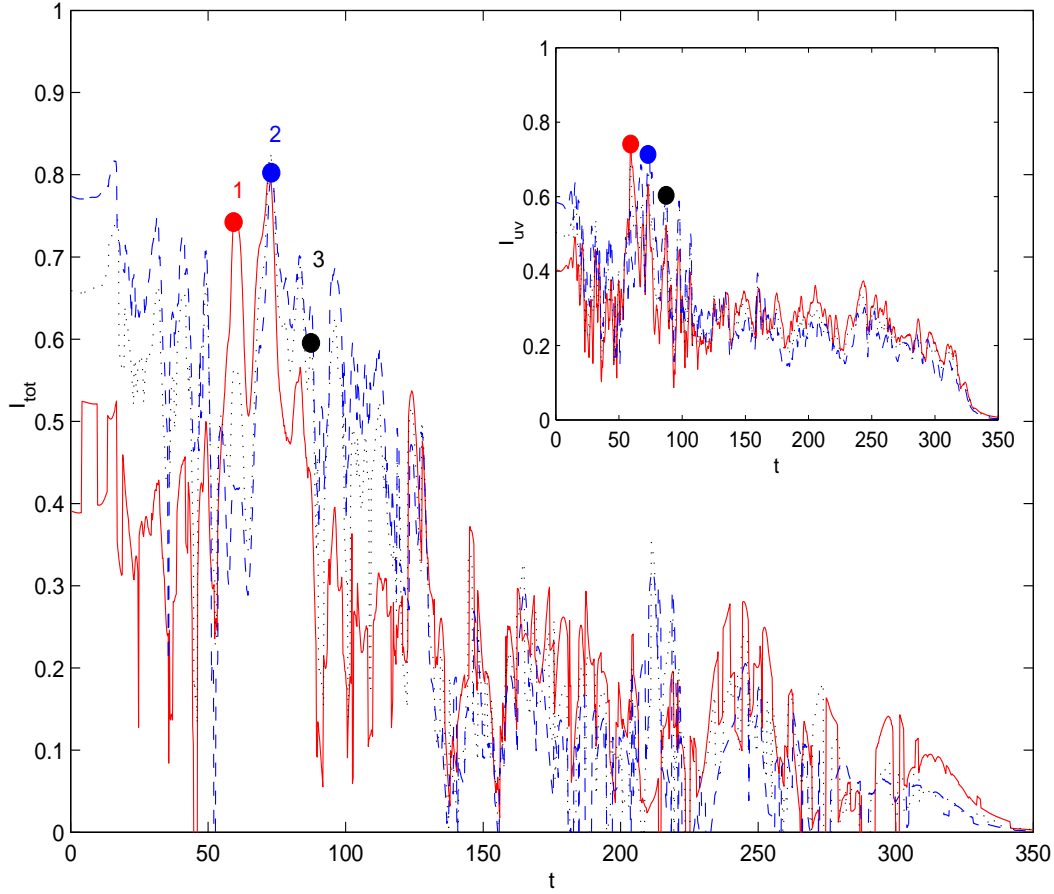


Figure 11. I_{tot} and I_{uv} (inset) as a function of time for TW s 3b₂:5 (red solid line), 3c₂:5 (black dotted line) and 3j₂:5 (blue dashed line) starting at TW 3b₃:125. The dots label the time of closest visits (numbers correspond to points in figure 10).

time: see figures 17 and 18. There is a clear positive correlation between I_{tot} and I_{uv} and significant evidence for recurrent TW visits. Comparing the two pdfs, there are a lot of close visits during the interval after the initial transient but before the rotational symmetry class of the flow changes. This is presumably the result of the flow percolating out of the specific TW region in which it is initially inserted. As a result, the pdf from data set A is likely to overestimate the visit frequency.

Using the criterion that a visit occurs if $I_{\text{tot}} > \epsilon$ & $I_{\text{tot}} + I_{\text{uv}} > 2$, the percentage visit time is plotted against the quality of the visit in Figure 19. To assess how close a visit needs to be – i.e. what ϵ is required – to be able to predict the instantaneous wall shear stress, Figures 20 and 21 plot the instantaneous DNS wall stress (over the matching wavelength) against the wall shear stress associated with the visited TW for

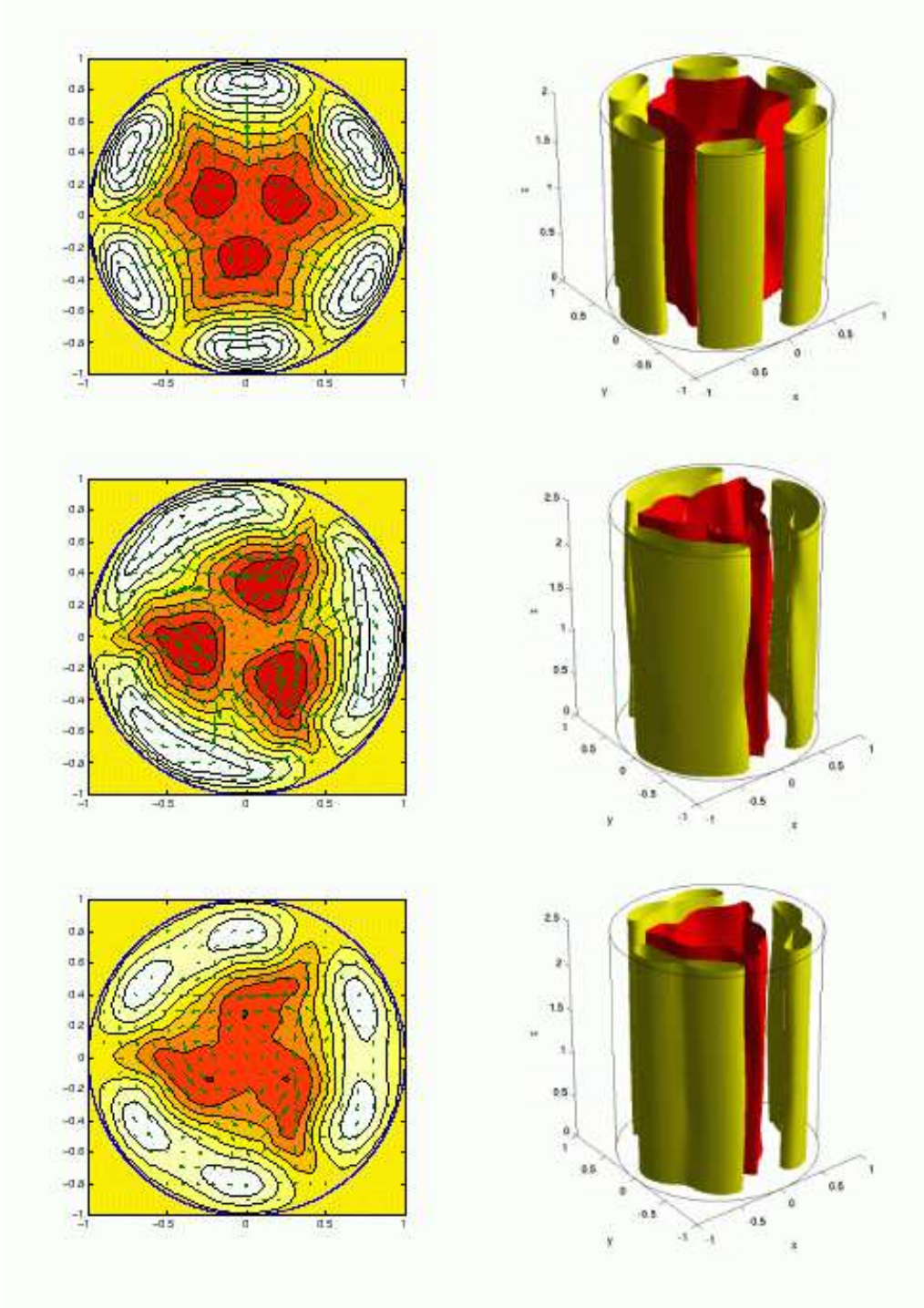


Figure 12. Comparison plots of the starting TW $3b_3:125$ (top), the DNS flow (middle) and the TW $3b_2:5$ (bottom) at point 1 in Figure 11. The left column shows the velocity field at a slice where the DNS flow most matches $3b_2:5$. The shading represents the axial velocity perturbation from laminar flow, with contours from -0.55 (dark) to 0.65 (light) (top), -0.55 to 0.5 (middle), and -0.55 to 0.35 (bottom), with a step of 0.15 . The arrows indicate the cross stream velocity, scaled on magnitude (maximum $0.135U$). The right column shows the axial structure over a wavelength. Two contours of the axial velocity are shown at $0.3U$ (light/dark).

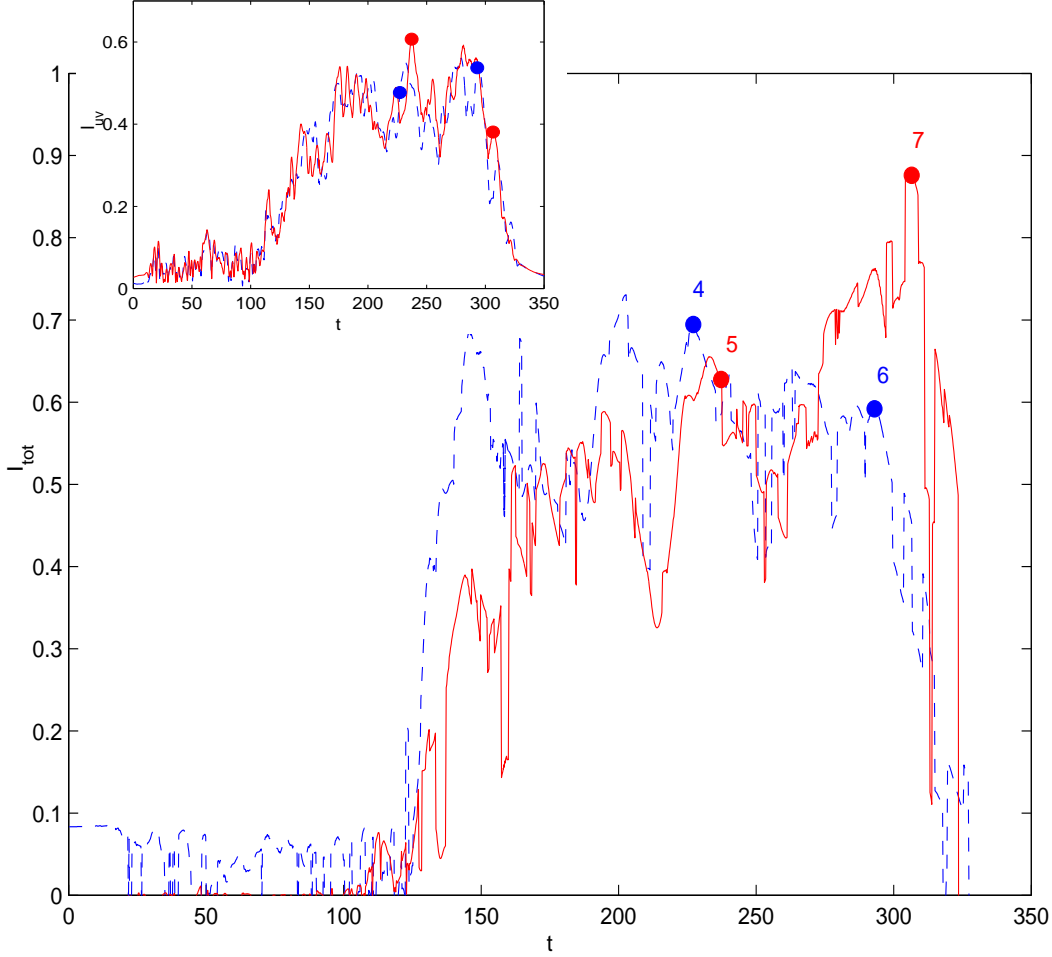


Figure 13. I_{tot} and I_{uv} (inset) as a function of time for TW s 2a_1:25 (blue dashed line) and 2b_1:875 (red solid line) starting at TW 3b_3:125. The dots label the times of closest visits (numbers correspond to points in figure 10).

three different values of β . The choice of seeking maximal I_{tot} to identify the closest TW was taken to facilitate the comparison as this should provide the best match between the DNS streak structure at the pipe wall with that of the TW. Even with this, the correlation results for set A indicate that only $\beta = 0.7$ level visits are really good enough to start making predictions of the wall shear stress from the visited TW. Since there are no $\beta = 0.7$ visits in set B, $\beta = 0.6$ is used to indicate closer visits and better stress correlation is evident at this level compared to the $\beta = 0.5$ results. Since the abscissa is discretized over the 37 TW values, each vertical strip of data in these figures indicates that that TW has been visited. Interestingly, Figure 20 shows a visit bias to TW s with larger wall stress ($\beta = 0.6$ $U^2 = Re$) whereas Figure 21 is oppositely skewed ($\beta = 0.6$ $U^2 = Re$) to lower wall stress TW s. A possible explanation for this is set A is dominated in a 2-to-1 ratio with runs started by upper branch TW s compared to lower

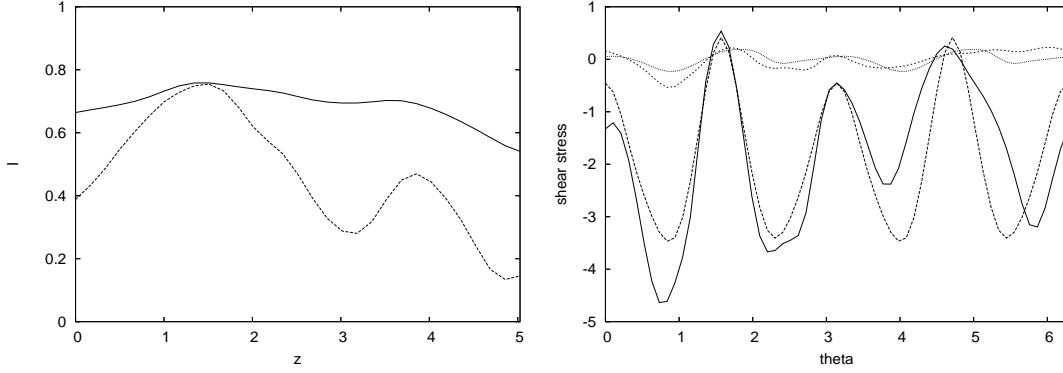


Figure 14. The left plot shows the correlations I_{tot} (upper line) and I_{uv} (lower line) over one wavelength of TW $2a_1:25$ at point 4 in Figure 13. The right plot shows the azimuthal distribution of the wall shear stress in units of $2 U^2 = Re$ at the axial position of maximum I_{tot} and I_{uv} near $z = 1.5$. The upper lines correspond to the azimuthal stress and the lower lines to axial stress (minus the laminar value of 4). The regular lines with 2-fold symmetry are for the TW and the more irregular ones from the DNS solution.

branch TWs. In the initial adjustment phase where the flow trajectory gradually leaves the vicinity of the initial TW, the flow visits other TWs and these are more likely to be upper rather than lower branch solutions in the neighbourhood of an initial upper branch solution. The reason lower branch TWs feature more in set B may be because the turbulent episodes considered were not long enough to desensitise the visit statistics from the initial relaxation process where the flow preferentially passes by lower branch TWs. This could indicate that efforts to remove this phase from the data but may not have been wholly successful.

Further runs were carried out in a $2 = 0.625 D$ ($10 D$) pipe in the search for more sustained turbulent data. Extending the spatial domain by a factor of 2 allows a whole new set of TW wavelengths to fit into the pipe, roughly doubling the number of allowed TWs. The correlation calculations were not extended to encompass this enlarged set for two reasons. Firstly the new TWs are interspersed within the 5D set which already sample the available solutions well. Therefore the new TWs should have structures very similar to the existing TW set. Secondly, the increase in the numerical overhead: currently calculating the correlation functions takes around 50% of the CPU time. However to compensate for this omission, the visit frequencies based on half the admissible TWs could justifiably be doubled. Initial conditions were randomly selected from an apparently sustained coarse turbulent run and used in intermediate- and fine-grid runs: see Table 4. The statistics across the accumulated $5;865 D = U$ long intermediate grid turbulent data were similar to those across the accumulated $4;780 D = U$ long fine grid turbulent data so the sets were merged to give a one large data set over $10;000 D = U$ in duration. The joint pdf of $(I_{tot}; I_{uv})$ shown in Figure 24 resembles that from 5D data set B as does the wall stress comparison during visits shown in Figure 25. Again, the most visited TWs look to be those with lower wall stresses and essentially the same subset of TWs are visited closely – $2a_1:25$, $2b_1:875$ and $3b_2:5$ in 5D data compared to $2a_1:25$, $2b_1:875$, $3b_2:5$ and $3c_3:125$ in the 10D data. Figures 22 and 23 show an example of a visit to $2a_1:25$ during a typical turbulent episode in these suite of runs. Significantly, no 4-fold symmetric

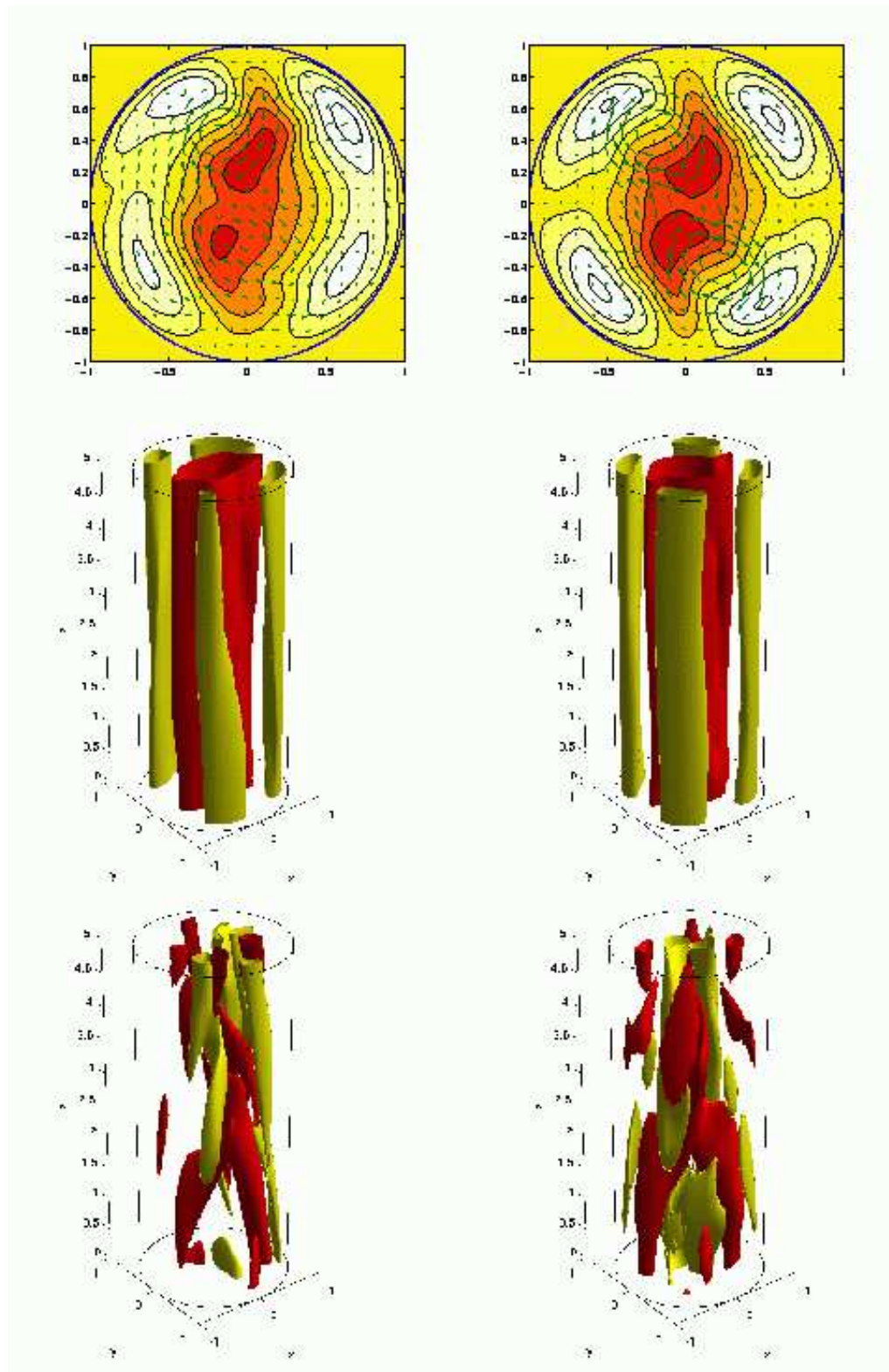


Figure 15. Comparison plots of the DNS flow (left column) and the TW 2a.125 (right column) at point 4 in figure 13. The top row shows the velocity fields at the streamwise position of maximum I_{tot} shown in figure 14 ($z = 1.5$). The shading represents the axial velocity perturbation from laminar flow with contours from -0.55 (dark) to 0.5 (light), with a step of 0.15 . The arrows indicate the cross stream velocity, scaled on magnitude (maximum $0.098U$). The middle row shows the streak structure over the wavelength of the TW, with contours of axial velocity at $0.3U$ (light/dark). The bottom row shows the axial vorticity, with contours at $0.8U=D$ (light/dark).

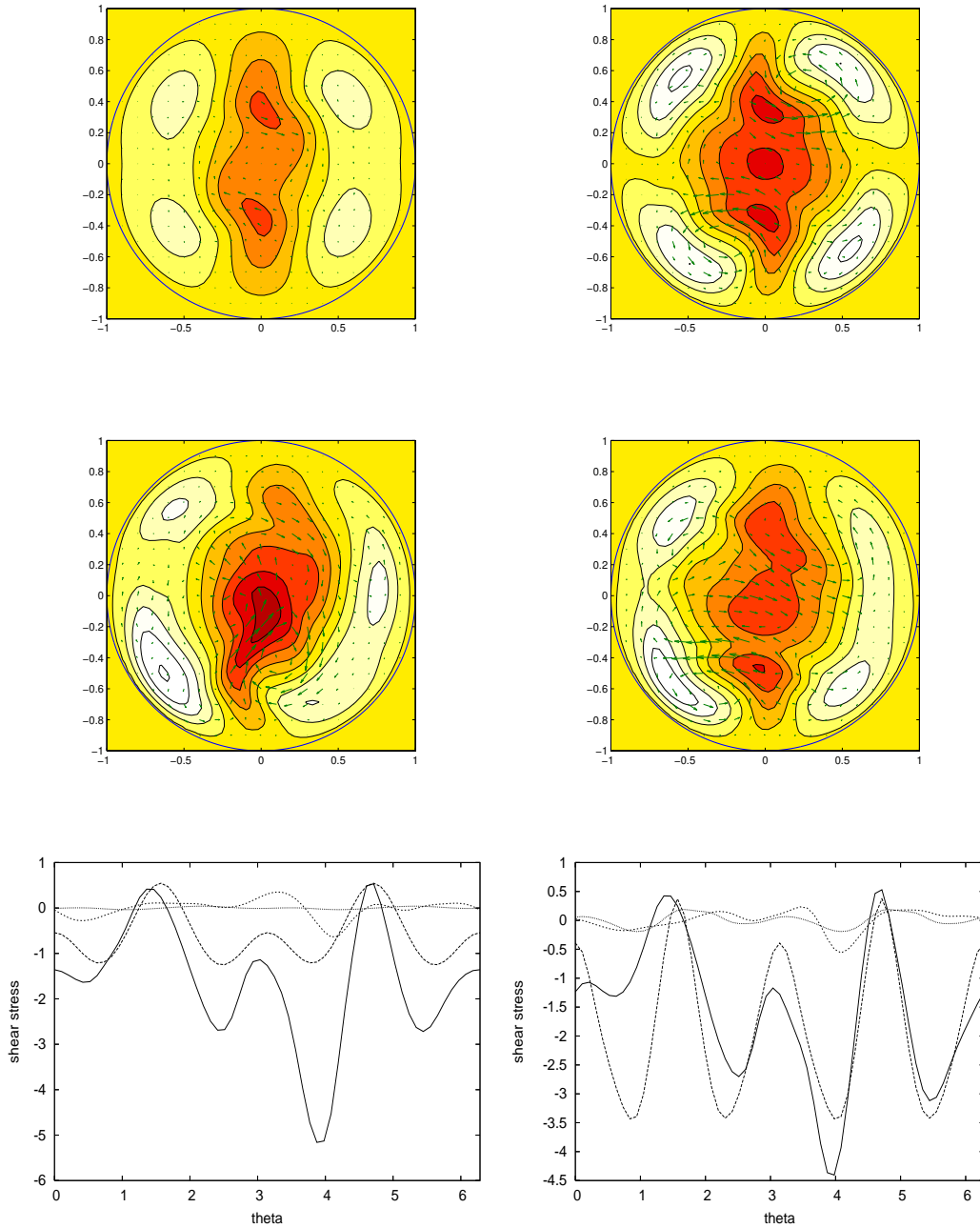


Figure 16. Comparison of the flow at point 5 in Figure 10 with TW 's 2b.1875 (left) and 2a.125 (right). The top row shows the velocity fields for the TW 's at the streamwise position of maximum correlation, the middle row the DNS flow, and the bottom row the wall shear stress at the same position. The shading represents the axial velocity perturbation from laminar flow with contours from -0.55 (dark) to 0.5 (light) (right column), -0.4 to 0.2 (top left), and -0.7 to 0.65 (middle left), with a step of 0.15. The arrows indicate the cross stream velocity, scaled on magnitude (maximum 0.162 U). For the wall shear stress, the top lines show the azimuthal stress (in units of $2 U^2 = Re$), and the bottom lines axial stress (minus the laminar value of 4). The regular lines with 2-fold symmetry are for the TW 's and the more irregular lines are from the DNS solution.

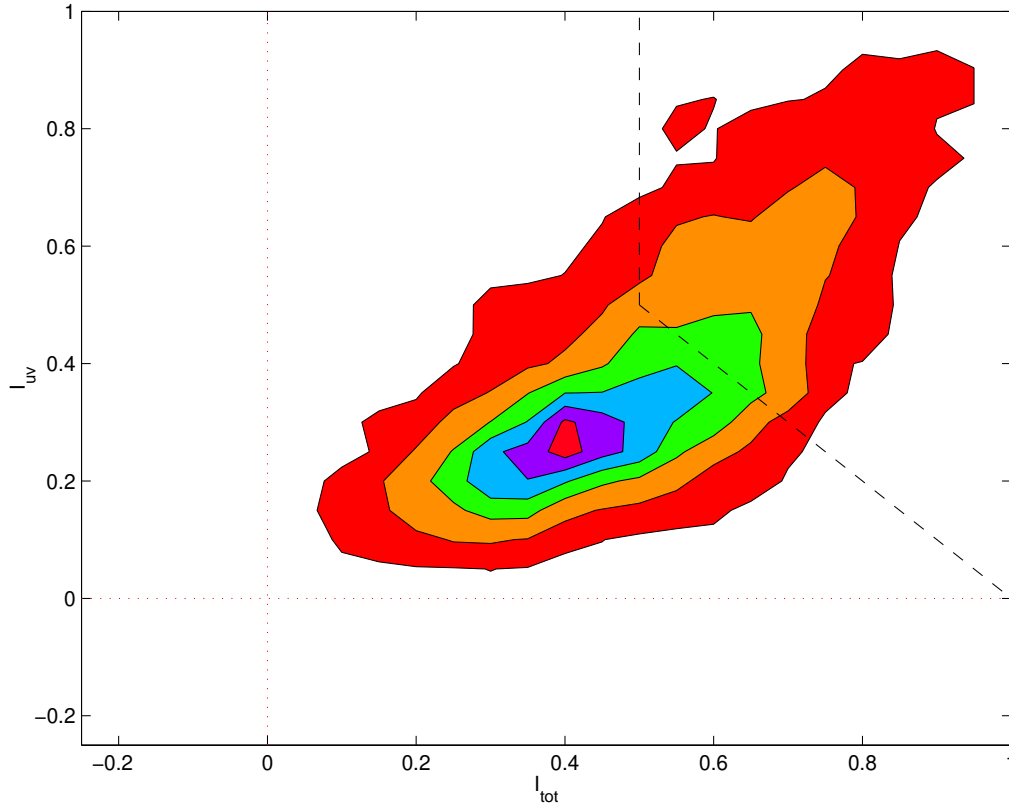


Figure 17. Joint pdf of I_{tot} and I_{uv} calculated over the turbulent episodes of all 5D runs started at the 8 upper and lower branch TWs (the values of I_{tot} and I_{uv} at a given time are selected by finding the TW with largest value of I_{tot}). Contours are drawn at 0.1; 0.1; 0.3; 0.5; 0.7 and 0.9 of the maximum value. The dashed lines cordon off the visit region defined by $I_{tot} > 0.5$ & $I_{tot} + I_{uv} > 1$.

TWs were visited in the 10D runs reinforcing the observation made in the 5D work that these TWs are not in the same part of phase space as that populated by a turbulent flow.

Figure 19 brings together the results of the frequency analysis by comparing the visit percentage as a function of visit quality (ϵ) for the three data sets. Doubling the 10D frequency data (as only half the possible TWs are considered) brings the observed visit frequency more into line with the results from the 5D data set B at $\epsilon = 0.5$. Taken together, they suggest that TWs are visited for approximately 10% of the time in turbulent pipe flow. Using $I_{tot} > 0.5$ as the criterion for a visit would increase the frequency of visits, by, in effect, ignoring the cross-stream component of the flow and considering the streamwise (streak) structure only.

Figure 26 shows the perturbation kinetic energy and the mean wall shear stress for a 10D pipe for one of the intermediate and fine grid runs started from coarse grid turbulent data. This shows that the turbulent flow in this pipe is concentrated in a small patch of the KE space, with both grids occupying the same region of the space. The other intermediate and fine grid turbulent runs are also concentrated in this region. Coarse grid turbulent runs occupy a somewhat different region of the KE space with lower values

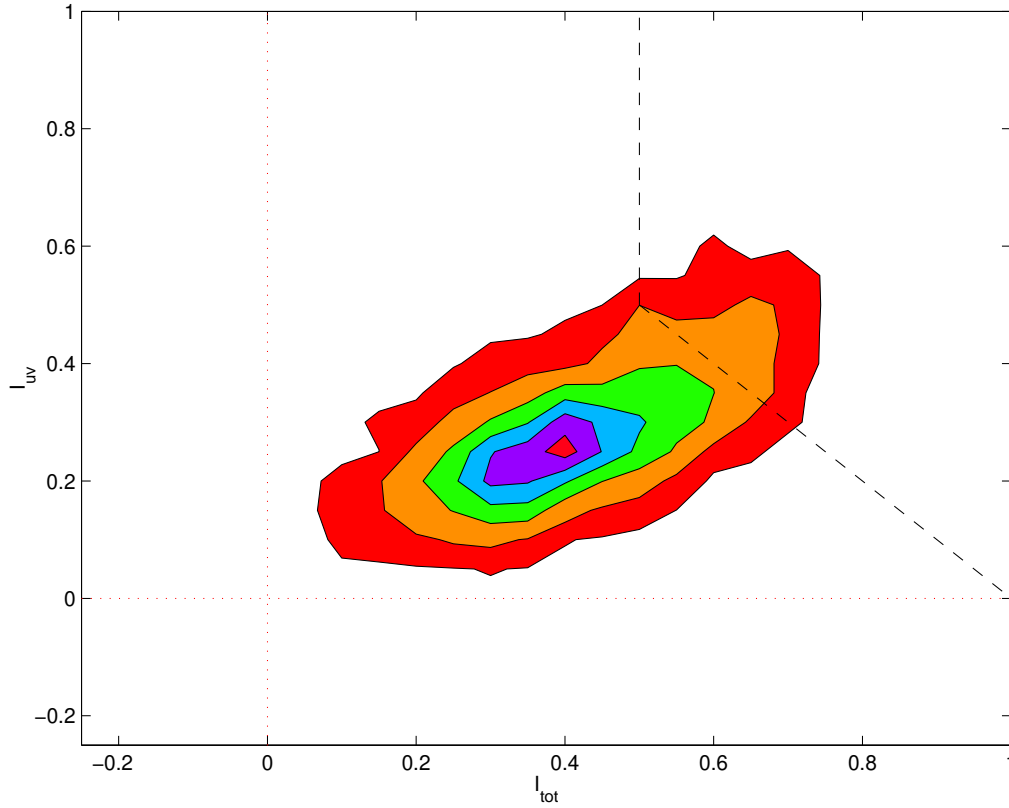


Figure 18. Joint pdf of I_{tot} and I_{uv} calculated over the turbulent episodes of all 5D runs started at the 8 upper and lower branch TWs using time episodes after the flow leaves the initial symmetry class (the values of I_{tot} and I_{uv} at a given time are selected by finding the TW with largest value of I_{tot}). Contours are drawn at 0.1; 0.3; 0.5; 0.7 and 0.9 of the maximum value. The dashed lines cordon off the visit region defined by $I_{tot} > 0.5$ & $I_{tot} + I_{uv} > 1$.

of both variables. Both the intermediate and fine grid have the same radial resolution ($N = 50$). A test run was performed with the same grid in r and z as the intermediate grid but an increased resolution in s ($N = 75$). Again, the flow occupied the same region in the KE space.

Figure 27 shows power spectra of the surplus kinetic energy and the wall shear stress for turbulent flow in a 10D pipe. The spectra were generated by taking the data for the four longest fine grid runs that were started from coarse grid turbulent data, with a sample time of $782.1 D = U$. A Hanning window was applied, with the windowed data scaled so that the variance matches that of the original data, and the spectra were generated by averaging over the four samples. Interestingly, the spectra show a peak, corresponding to a period of approximately $98 D = U$ which suggests a periodic orbit embedded in the turbulent dynamics. This is currently under investigation.

The intermediate grid data produced spectra consistent with those for the fine grid, while the coarse grid also produced a peak, but at a higher frequency.

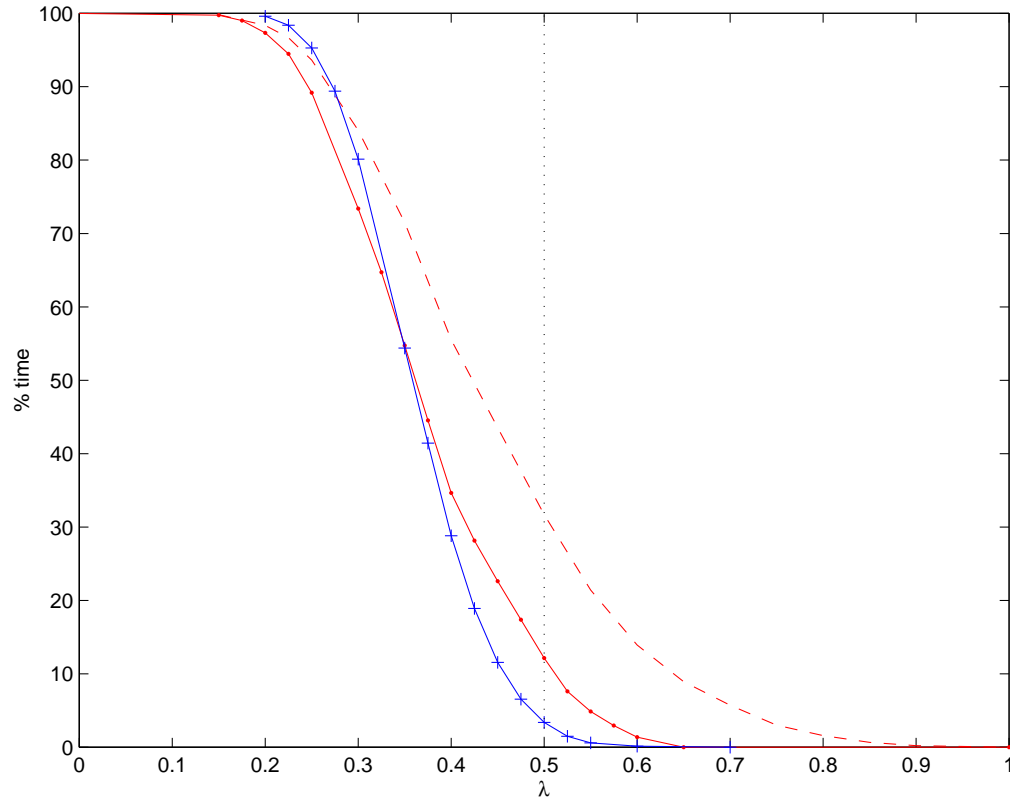


Figure 19. The percentage of time a turbulent flow ‘visits’ a TW based on the criterion $I_{tot} >$ and $I_{tot} + I_{uv} > 2$ as a function of λ . Statistics gathered from the 5D runs started at a TW with a) only the initial transient subtracted (dashed red line) and b) considering only times where the flow has left the initial symmetry class of the TW (solid red line with dots on), together with turbulent data compiled from various runs at 10D (blue solid line with crosses on).

4. Discussion

At this point it is worth cataloguing the achievements of this investigation.

(a) Using the travelling waves already known as starting points, all travelling wave solutions (TWs) of varying wavelengths and azimuthal symmetries which exist at $Re = 2400$ have been traced out (Figures 1 and 2). They naturally partition into 3 distinct classes of particular rotational symmetry about the axis – 2-fold, 3-fold and 4-fold symmetric TWs – and 37 in total fit into a ≈ 0.625 (5)D periodic pipe.

(b) The linear stability of four ‘lower branch’ TWs (TWs with some of the lowest wall stresses of the 37) and four ‘upper branch’ solutions (TWs with some of the highest wall stresses of the 37) has been carried out. All are inertially unstable and therefore saddles in phase space with growth rates typically of the size $O(0.1 U/D)$ and all have very low dimensional unstable manifolds.

(c) All the lower branch solutions considered appear to sit on a surface which separates initial conditions which uneventfully relax and those which lead to a turbulent-looking evolution. In contrast, initial conditions near all the upper branch solutions tested

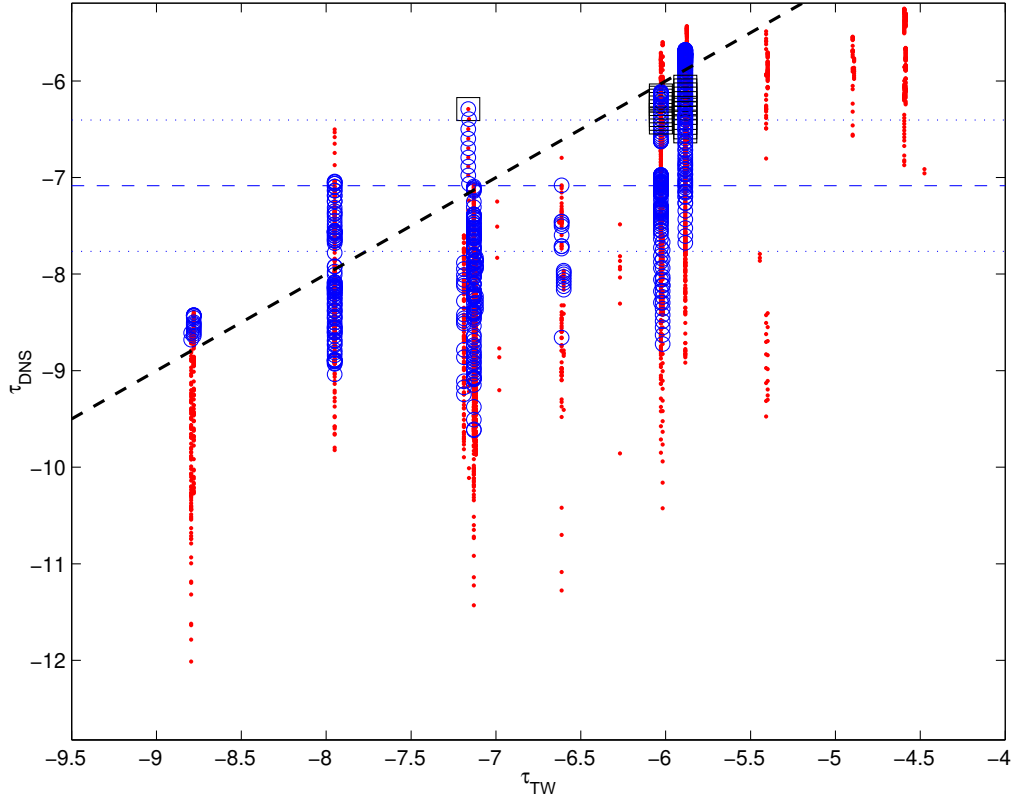


Figure 20. A plot of the wall shear stress τ_{DNS} versus the wall shear stress τ_{TW} of the TW being visited (τ_{DNS} is measured across the matching wavelength of the TW) for the 5D data set A runs. The visit criterion is $I_{tot} > \epsilon$ & $I_{tot} + I_{uv} > 2$, where $\epsilon = 0.5$ (red dots) indicate approximate visits, $\epsilon = 0.7$ (blue circles) close visits and $\epsilon = 0.9$ (black squares) very close visits. The thick (black) diagonal dashed line indicates a perfect match $\tau_{DNS} = \tau_{TW}$. The horizontal (blue) dashed line is the mean wall shear stress across the whole pipe, the dotted lines indicate one standard deviation either side of this mean and the limits of the vertical axis have been set to the maximum (-12.8) and minimum (-5.2) wall shear stress values (in units of $2 U^2 = Re$). Each vertical strip of points represents one TW – the close visits only occur for upper branch solutions where $\tau_{TW} < -5.2$.

invariably become turbulent.

(d) Turbulence in a 5D periodic pipe at $Re = 2400$ may be long-lived but ultimately appears only transient. Turbulence also seems transient in a 10D pipe at $Re = 2400$ but the transients have, on average, a longer life. The mean lifetime of a turbulent episode is sensitive to the numerical resolution used, with turbulence appearing to last longer, if not sustained, in underresolved calculations.

(e) A number of different correlation functions were experimented with to measure how ‘close’ a given velocity field is to a TW. Two, I_{tot} and I_{uv} , were chosen and a visit criterion – $I_{tot} > \epsilon$ and $I_{tot} + I_{uv} > 2$ – developed based on a ‘quality of visit’ parameter. After examining the velocity matches at various different levels of ϵ , a value of 0.5 was taken as indicating a ‘visit’ with values of 0.6 and higher indicating a ‘close’ visit.

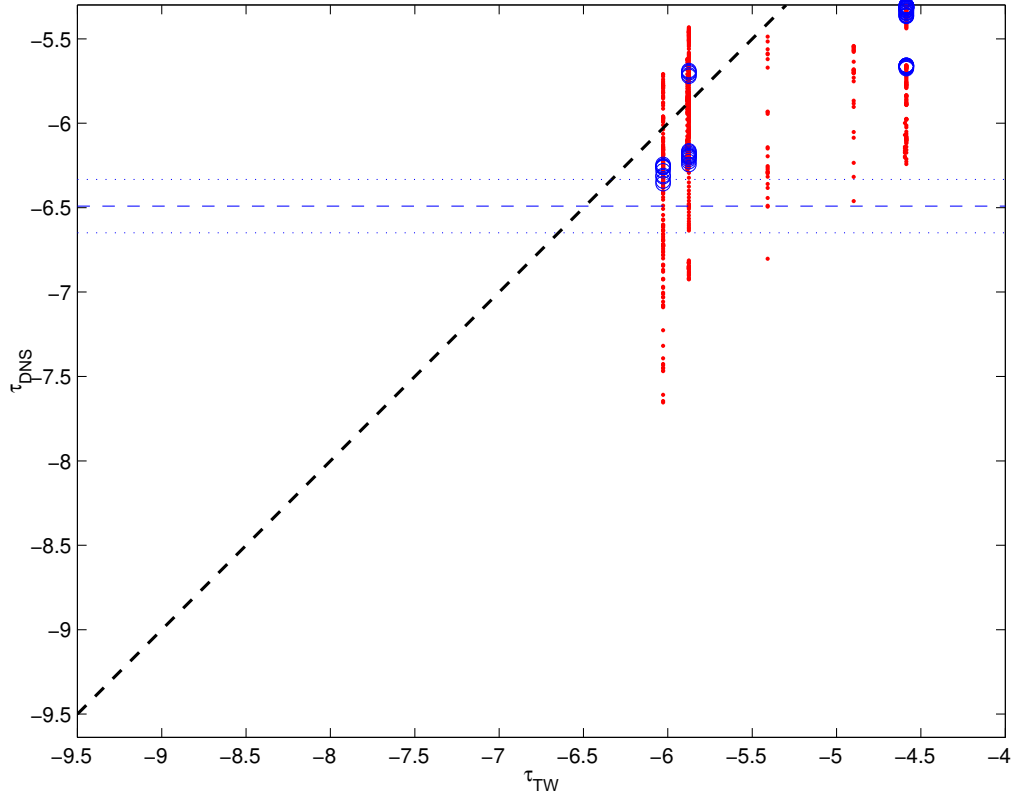


Figure 21. A plot of the wall shear stress τ_{DNS} versus the wall shear stress τ_{TW} of the TW being visited (τ_{DNS} is measured across the matching wavelength of the TW) for the 5D data set B runs. The visit criterion is $I_{tot} > \delta$ & $I_{tot} + I_{uv} > 2$, where $\delta = 0.5$ (red dots) indicate approximate visits, $\delta = 0.6$ (blue circles) close visits. There are no very close ($\delta = 0.9$) visits. The thick (black) diagonal dashed line indicates a perfect match $\tau_{DNS} = \tau_{TW}$. The horizontal (blue) dashed line is the mean wall shear stress across the whole pipe, the dotted lines indicate one standard deviation either side of this mean and the limits of the vertical axis have been set to the maximum (-9.6) and minimum (-5.3) wall shear stress values (in units of $2U^2/Re$). Each vertical strip of points represents one TW. For $\delta = 0.5$, the TWs visited are 2a.1:25, 2b.1:875, 3b.2:5, 3a.3:125 and 3c.3:125. The TWs closely visited ($\delta = 0.6$) are 2a.1:25, 2b.1:875 and 3b.2:5.

(f) Turbulent data in both 5D and 10D pipes indicate that some 2-fold and 3-fold symmetric TWs are recurrently visited while others are not. In particular, no evidence was found for visits to 4-fold symmetric TWs. The visited TWs correspond to low-to-intermediate wall stress solutions which are embedded in the same part of phase space as the turbulent dynamics. Other TWs are clearly in very different phase space locations and hence are never visited except if the flow is specifically inserted there initially (e.g. all the 4-fold TWs).

(g) Based on the correlation functions, I_{tot} and I_{uv} , used and the visiting criterion adopted ($\delta = 0.5$), numerical evidence suggests that travelling waves are only visited for about 10% of the time in turbulent pipe flow.

The last finding answers the original motivating question for this study. The fact that a turbulent flow is apparently visiting a TW only 10% of the time implies that it is

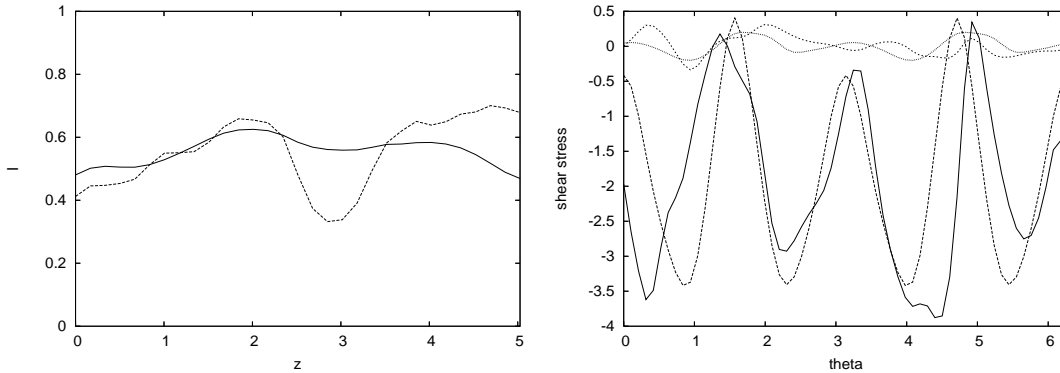


Figure 22. The left plot shows the correlations I_{tot} (solid line) and I_{uv} (dashed line) over one wavelength of TW $2\pi/1.25$ for a fine grid 10D pipe starting from a coarse grid turbulent flow. The right plot shows the azimuthal distribution of the wall shear stress in units of $2 U^2 = Re$ at the axial position of maximum $I_{tot} + I_{uv}$ near $z = 1.84$. The upper lines correspond to the azimuthal stress and the lower lines to axial stress (minus the laminar value of -4). The regular lines with 2-fold symmetry are for the TW and the more irregular ones from the DNS values.

of limited use to view turbulence as the random switching between the neighbourhoods of TWs. From the perspective of, say, predicting the average turbulent wall stress, an appropriately weighted sum of all the relevant TW wall stresses seems unlikely to work given that so much time is spent away from the TWs in phase space. The fact that even during a visit, the match between the flow's wall stress and that of the TW can be poor is further cause for pessimism. The way out of this conclusion, of course, is that other phase space objects such as periodic orbits – perhaps glimpsed in figure 27 – need to be included in any such expansion. The results presented here indicate just how important these missing objects are given the low visit times for the TWs and the next challenge to isolate them seems clear.

RRK acknowledges the support of EPSRC under grant GR/S76144/01.

REFERENCES

- Artuso, R., Aurell, E. & Cvitanovic, P. 1990a Recycling of strange sets: I cycle expansions. *Nonlinearity* 3, 325{360.
- Artuso, R., Aurell, E. & Cvitanovic, P. 1990b Recycling of strange sets: II applications. *Nonlinearity* 3, 361{.
- Clever, R. M. & Busse, F. H. 1992 Three-dimensional convection in a horizontal fluid layer subjected to a constant shear. *J. Fluid Mech.* 234, 511{527.
- Clever, R. M. & Busse, F. H. 1997 Tertiary and quaternary solutions for plane couette flow. *J. Fluid Mech.* 344, 137{153.
- Cvitanovic, P. 1988 Invariant measurement of strange sets in terms of cycles. *Phys. Rev. Lett.* 61, 2729{2732.
- Eckhardt, B., Faisst, H., Schmieg, A. & Schumacher, J. 2002 Turbulence transition

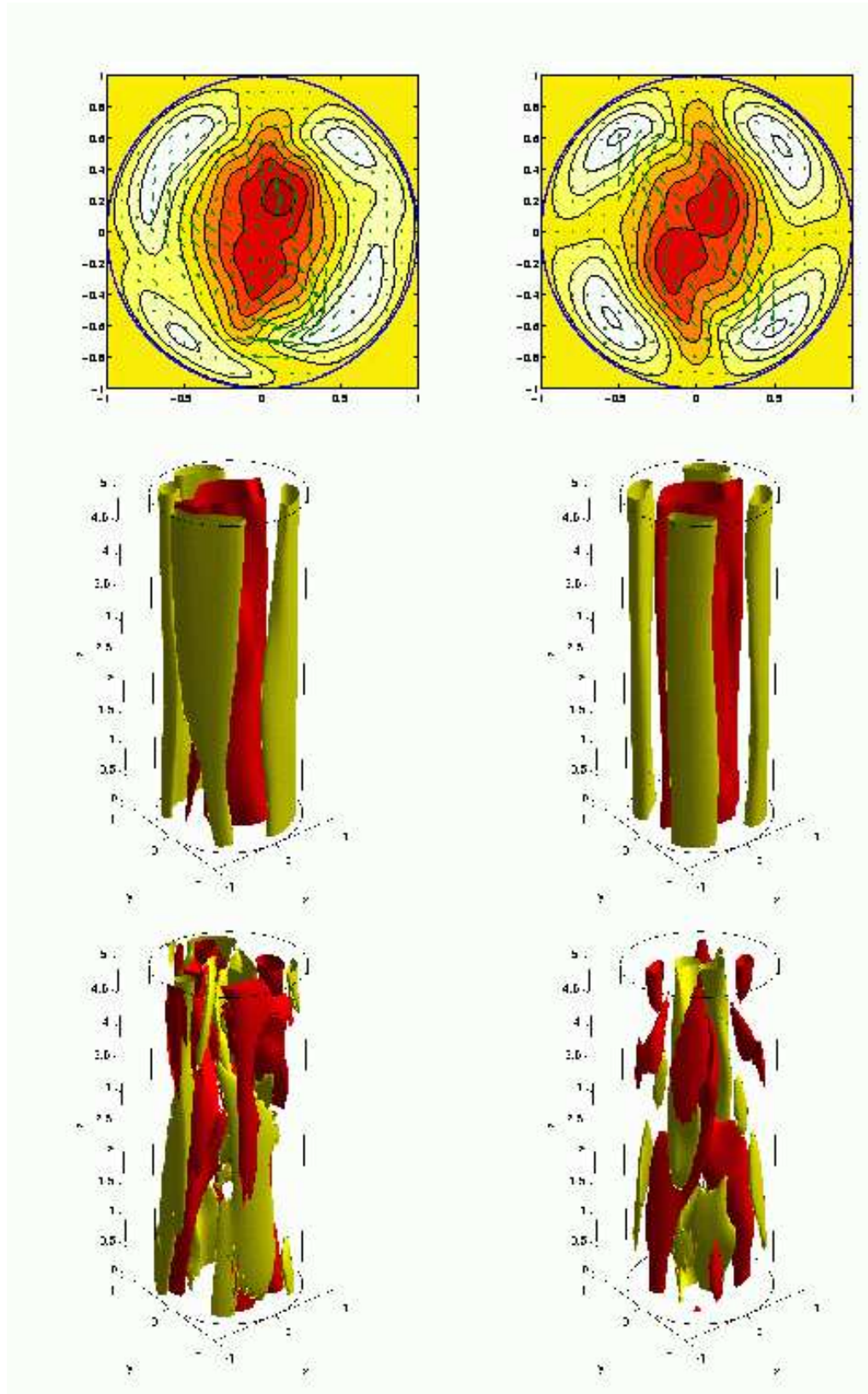


Figure 23. Comparison plots of the DNS flow (left column) and the TW $2a_{1.25}$ (right column) captured during a turbulent fine grid run in a 10D pipe. The top row shows the velocity fields at the streamwise position of maximum $I_{tot} + I_{uv}$ shown in figure 22 ($z = 1.84$). The shading represents the axial velocity perturbation from laminar flow with contours from -0.7 (dark) to 0.35 (light) for the DNS, and -0.55 to 0.5 for the TW, with a step of 0.15. The arrows indicate the

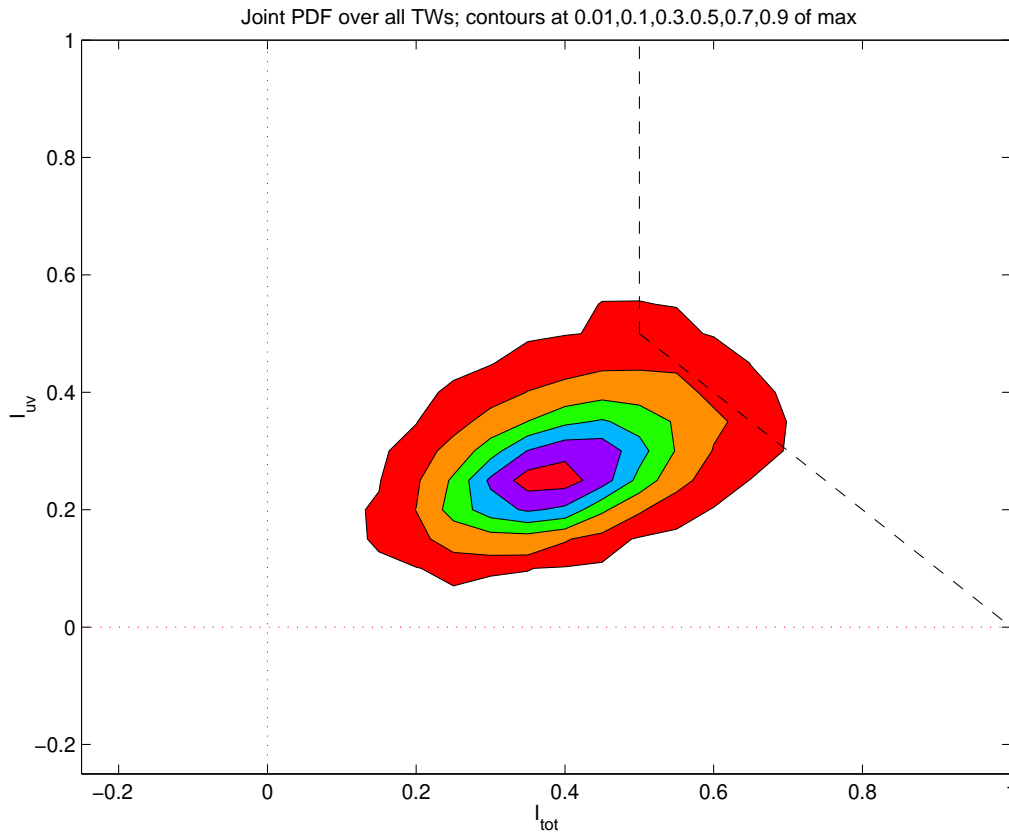


Figure 24. Joint pdf of I_{tot} and I_{uv} calculated over the turbulent episodes of all 10D runs (the values of I_{tot} and I_{uv} at a given time are selected by finding the TW with largest value of I_{tot}). Contours are drawn at 0.01;0.1;0.3;0.5;0.7 and 0.9 of the maximum value. The dashed lines cordon off the visit region defined by $I_{tot} > 0.5$ & $I_{tot} + I_{uv} > 1$.

in shear flows. *Advances in Turbulence IX: Proceedings of the Ninth European Turbulence Conference, Barcelona* edited by I.P. Castro, P.E. Hancock and T.G. Thomas p. 701.

Eckhardt, B., Schneider, T., Hof, B. & Westerweel, J. 2007 Turbulence transition in pipe flow. *Annual Review of Fluid Mechanics* – submitted.

Eggels, J.G.M., Unger, F., Weiss, M.H., Westerweel, J., Adrian, R.J., Friedrich, R. & Nieuwstadt, F.T.M. 1994 Fully developed turbulent pipe flow: a comparison between direct numerical simulation and experiment. *J. Fluid Mech.* 268, 175{209.

Faisst, H. & Eckhardt, B. 2003 Traveling waves in pipe flow. *Phys. Rev. Lett.* 91, 224502.

Faisst, H. & Eckhardt, B. 2004 Sensitive dependence on initial conditions in transition to turbulence in pipe flow. *J. Fluid Mech.* 504, 343{352.

Hof, B., van Doorne, C.W.H., Westerweel, J., Nieuwstadt, F.T.M., Faisst, H., Eckhardt, B., Wedin, H., Kerswell, R.R. & Waleffe, F. 2004 Experimental observation of nonlinear traveling waves in turbulent pipe flow. *Science* 305, 1594{1597.

Hof, B., van Doorne, C.W.H., Westerweel, J. & Nieuwstadt, F.T.M. 2005 Turbulence regeneration in pipe flow at moderate Reynolds numbers. *Phys. Rev. Lett.* 95, 214502.

Hof, B., Westerweel, J., Schneider, T.M. & Eckhardt, B. 2006 Finite lifetime of turbulence in shear flows. *Nature* 443, 59{62.

Itano, T. & Toh, S. 2001 The dynamics of bursting process in wall turbulence. *J. Phys. Soc. Japan* 70, 703{716.

Jimenez, J., Kawahara, G., Simens, M.P., Nagata, M. & Shiba, M. 2005 Characterization

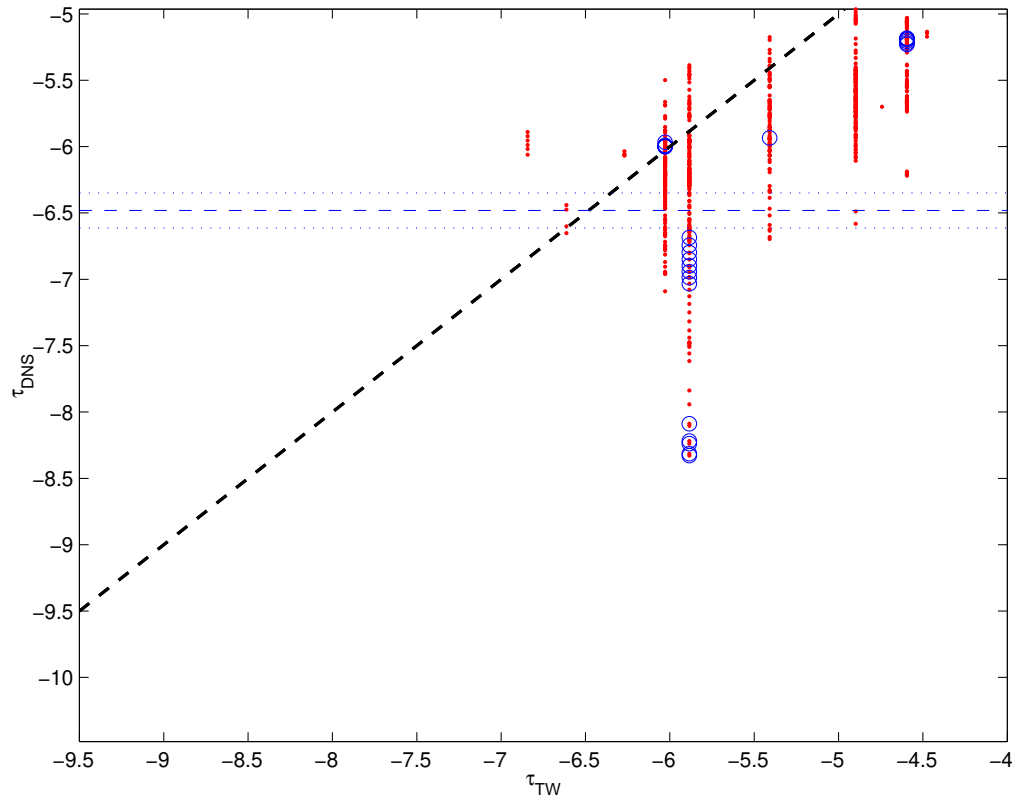


Figure 25. A plot of the wall shear stress τ_{DNS} versus the wall shear stress τ_{TW} of the TW being visited (τ_{DNS} is measured across the matching wavelength of the TW) for the 10D runs. The visit criterion is $I_{tot} > \epsilon$ & $I_{tot} + I_{uv} > 2$, where $\epsilon = 0.5$ (red dots) indicates approximate visits and $\epsilon = 0.6$ (blue circles) closer visits (there are no $\epsilon = 0.7$ visits). The thick (black) diagonal dashed line indicates a perfect match $\tau_{DNS} = \tau_{TW}$. The horizontal (blue) dashed line is the mean wall shear stress across the whole pipe, the dotted lines indicate one standard deviation either side of this mean and the limits of the vertical axis have been set to the maximum (-10.48) and minimum (-4.96) wall shear stress values (in units of $2 U^2 = Re$). Each vertical strip of points represents one TW. For $\epsilon = 0.5$, the TWs visited are 2a.1.25, 2b.1.25, 3c.1.25, 2a.1.875, 2b.1.875, 3c.1.875, 3b.2.5, 3c.2.5, 3d.2.5, 3a.3.125 and 3c.3.125. The TWs closely visited ($\epsilon = 0.6$) are 2a.1.25, 2b.1.875, 3b.2.5 and 3c.3.125.

of near-wall turbulence in terms of equilibrium and bursting solutions. *Phys. Fluids* 17, 015105.

Jimenez, J. & Simens, M. P. 2001 Low-dimensional dynamics in a turbulent wall flow. *J. Fluid Mech.* 435, 81.

Kawahara, G. & Kida, S. 2001 Periodic motion embedded in plane Couette turbulence: regeneration cycle and burst. *J. Fluid Mech.* 449, 291-300.

Kerswell, R. R. 2005 Recent progress in understanding the transition to turbulence in a pipe. *Nonlinearity* 18, R17-R44.

Nagata, M. 1990 Three-dimensional finite-amplitude solutions to plane Couette flow: Bifurcation from laminarity. *J. Fluid Mech.* 217, 519.

Nikitin, N. 2006 Third-order-accurate semi-implicit Runge-Kutta scheme for incompressible Navier-Stokes equations. *Int. J. Numer. Meth. Fluids* 51, 221-233.

Peixinho, J. & Mullin, T. 2006 Decay of turbulence in pipe flow. *Phys. Rev. Lett.* 96, 094501.

Schlichting, H. 1968 Boundary layer theory. McGraw-Hill, New York.

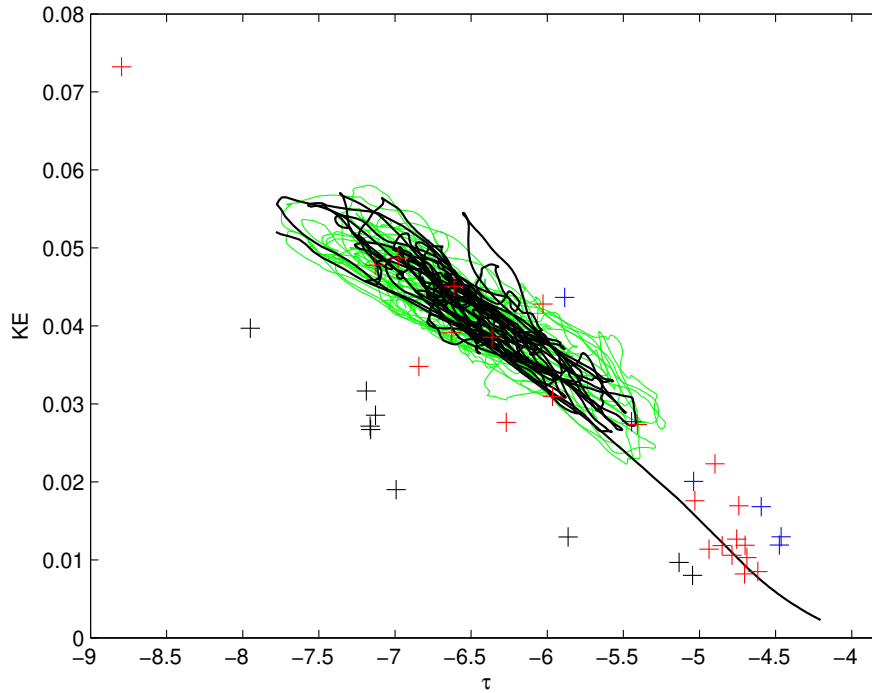


Figure 26. The surplus kinetic energy per unit mass, $\frac{1}{2}(\mathbf{u} - \mathbf{u}_{\text{lam}})^2$, in units of U^2 versus wall shear stress in units of $2U^2 = \text{Re}$ for u_{DNS} for two 10D runs started from a coarse grid turbulent run. The green line is for an intermediate (50,48,80) grid run and the black line a fine (50,60,120) grid run. The laminar state is represented by the point $(-4;0)$. All the TWs are also plotted: blue for 2-fold TWs, red for 3-fold TWs, and black for 4-fold TWs.

- Schmiegel, A. & Eckhardt, B. 1997 Fractal stability border in plane Couette flow. *Phys. Rev. Lett.* 277, 197{225.
- Skufca, J., Yorke, J.A. & Eckhardt, B. 2006 The edge of chaos in a parallel shear flow. *Phys. Rev. Lett.* 96, 174101.
- Toh, S. & Itano, T. 2003 A periodic-like solution in channel flow. *J. Fluid Mech.* 481, 67{76.
- van Veen, L., Kida, S. & Kawahara, G. 2006 Periodic motion representing isotropic turbulence. *Fluid Dynamics Research* 38, 19{46.
- Waleffe, F. 1998 Three dimensional coherent states in plane shear flows. *Phys. Rev. Lett.* 81, 4140{4143.
- Waleffe, F. 2001 Exact coherent structures in channel flow. *J. Fluid Mech.* 508, 333{371.
- Waleffe, F. 2003 Homotopy of exact coherent structures in plane shear flows. *Phys. Fluids* 15, 1517{1534.
- Wedin, H. & Kerswell, R. R. 2004 Exact coherent structures in pipe flow: travelling wave solutions. *J. Fluid Mech.* 508, 333{371.
- Willis, A. P. & Kerswell, R. R. 2006 Critical behaviour in the relaminarisation of localised turbulence in pipe flow. *Phys. Rev. Lett.* in press.
- Wynanski, I. J. & Champagne, F. H. 1973 On transition in a pipe. part 1. the origin of pulses and slugs and the flow in a turbulent slug. *J. Fluid Mech.* 59, 281{351.

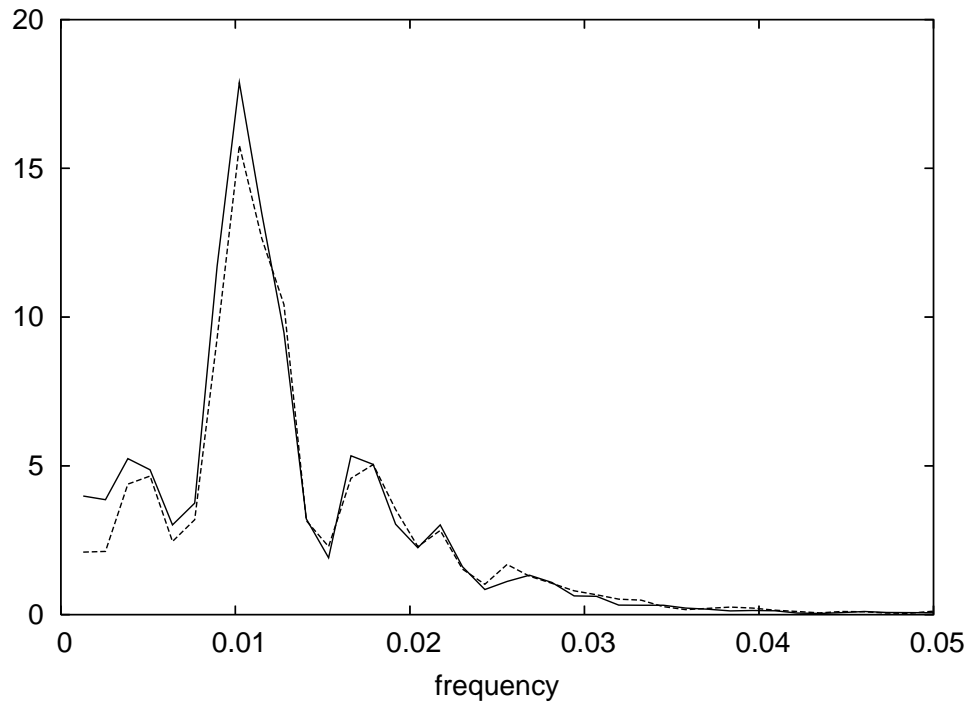


Figure 27. The power spectra of surplus kinetic energy (multiplied by 5000) in units of $U^3 D$ (dashed) and wall shear stress in units of $4UD = Re^2$ (solid) versus frequency. The maximum in the spectra corresponds to a period of approximately 98 in units of $D = U$.

TW	run	1	2	3	4	5	6	7	8	9	10	11	12
2a_0:625													
2b_0:625													
2a_1:25							?	?					
2b_1:25		?											
2a_1:875													
2b_1:875													
3a_1:25													
3b_1:25													
3c_1:25													
3a_1:875													
3b_1:875													
3c_1:875													
3d_1:875													
3e_1:875													
3a_2:5				?									
3b_2:5													
3c_2:5													
3d_2:5													
3e_2:5													
3f_2:5													
3g_2:5													
3h_2:5					?								
3j_2:5										?	?		
3a_3:125													
3b_3:125								?	?				
3c_3:125													
3d_3:125													
3e_3:125													
4a_2:5													
4b_2:5													
4c_2:5													
4a_3:125													
4b_3:125					?								
4c_3:125											?	?	
4d_3:125													
4e_3:125													
4f_3:125													

Table 2. Summary of visits for the 12 transitional runs (4 starting at lower branch TW s + 8 starting at upper branch TW s) which have turbulent episodes (data set A). TW s visited using the criterion $I_{tot} = 0.5$ & $I_{tot} + I_{uv} = 1$ at least once in a given run have the symbol entered under that column against them (? indicates the starting TW). A indicates where the higher threshold of $I_{tot} = 0.6$ & $I_{tot} + I_{uv} = 1.2$ is satisfied. The initial transient as the flow moves away from the starting TW – typically of $O(30D/U)$ duration – is not considered. The code for the run numbers is: 1 – 2b_1:25() (where () indicates the sign of the eigenfunction perturbation), 2 – 3a_2:5(+), 3 – 3h_2:5(+), 4 – 4b_3:125(+), 5 & 6 – 2a_1:25(=), 7 & 8 – 3b_3:125(=), 9 & 10 – 3j_2:5(=), 11 & 12 – 4c_3:125(=).

TW	run	1	2	3	4	5	6	7	8	9	10	11	12
2a_0:625			0.83			0.86		0.98	0.86				
2b_0:625		0.79	0.91			0.91		0.89	0.87				
2a_1:25						?	?		0.89				
2b_1:25		?	0.81	0.94			0.95						
2a_1:875			0.91			0.88			0.75	0.87			
2b_1:875						0.92			0.86	0.97	0.95		
3a_1:25													
3b_1:25													
3c_1:25													
3a_1:875			0.77										
3b_1:875													
3c_1:875													
3d_1:875													
3e_1:875													
3a_2:5			?		0.86		0.96				0.71		
3b_2:5		0.89		0.91	0.98				0.88		0.85		
3c_2:5					0.87	0.85							
3d_2:5				0.75							0.95		
3e_2:5													
3f_2:5													
3g_2:5							0.73						
3h_2:5			0.90	?	0.83		0.93						
3j_2:5					0.83					?	?		
3a_3:125				0.88		0.88					0.97		
3b_3:125								?	?				
3c_3:125		0.87		0.90		0.86					0.87		
3d_3:125													
3e_3:125													
4a_2:5													
4b_2:5													
4c_2:5													
4a_3:125													
4b_3:125					?								
4c_3:125											?	?	
4d_3:125													
4e_3:125													
4f_3:125													

Table 3. As for Table 2 except now only times when the row has left the symmetry class of the starting TW are considered (data set B). Also numerical values are recorded of $I_{\text{tot}} + I_{\text{uv}}$ in all near-miss instances where $I_{\text{tot}} > 0.5$ but a \quad ($= 0.5$) or \quad ($= 0.6$) is not warranted.

Pipe Length	Run	Turbulent Duration in $D=U$	Initiation	Resolution ($N;M;K$)
5D	1	433 (673)	2b_1.25 ()	(50,60,60)
	2	327 (554)	3a_2.5 (+)	(50,60,60)
	3	340 (517)	3h_2.5 (+)	(50,60,60)
	4	147 (251)	4b_3.125 (+)	(50,60,60)
	5	195 (385)	2a_1.25 (+)	(50,60,60)
	6	397 (609)	2a_1.25 ()	(50,60,60)
	7	153 (265)	3b_3.125 (+)	(50,60,60)
	8	263 (400)	3b_3.125 ()	(50,60,60)
	9	90 (257)	3j_2.5 (+)	(50,60,60)
	10	18 (133)	3j_2.5 ()	(50,60,60)
10D	1	879	T	(50,48,80)
	2	1131	T	(50,48,80)
	3	390	T	(50,48,80)
	4	488	T	(50,48,80)
	5	349	T	(50,48,80)
	6	1446	T	(50,48,80)
	7	1182	T	(50,48,80)
	8	229	2b_1.25 (-)	(50,60,120)
	9	335	T	(50,60,120)
	10	390	T	(50,60,120)
	11	586	T	(50,60,120)
	12	642	T	(50,60,120)
	13	558	T	(50,60,120)
	14	265	T	(50,60,120)
	15	640	T	(50,60,120)
	16	1135	T	(50,60,120)

Table 4. This Table lists the various runs used to produce the 'visit' statistics. The 5D data comes from initiating the code with a disturbed TW and two 'turbulent' duration times are listed. The first is measured from when the flow leaves the initial symmetry class of the TW (used for data set B) whereas the second, larger figure (in parentheses) is based on when the correlation function for the starting TW stops decreasing which is a much weaker condition that occurs earlier (used for data set A). The 10D runs are almost exclusively started using randomly selected velocity fields from a long turbulent run generated using a coarse (25,32,60) grid (a strategy labelled as 'T' in the Table). Note that some of the 10D runs were still turbulent when this data was gathered, whereas all the 5D runs had relaminarised.